Western blotting. Cultured cells were washed with PBS buffer and lysed by freeze–thawing in ice-cold lysis buffer (50 mM Hepes, 1% Triton X-100, 10% glycerol, 150 mM NaCl, 100 mM NaF, 1.5 mM $MgCl_2$, 1 mM ECTA, 1 mM Na_3VO_4, 1 mM PMSF, and 10 μg/mL aprotinin). After removal of nuclei and cellular debris by centrifugation at 12,000 rpm for 5 min at 4 °C, normalized lysate (40 μg) was electrophoresed on 12% SDS–polyacrylamide gels and transferred onto nitrocellulose filters. The filters were blocked overnight at 4 °C in TBS-T containing 5% non-fat milk powder and then incubated for 1 h with 1:1000, diluted anti-human CXCR4 mouse monoclonal antibody (R&D Systems, Minneapolis, MN, USA) or 1:1000, diluted anti-human β-actin mouse monoclonal antibody (Sigma, St. Louis, MO, USA). The filters were incubated for 1 h with 1:4000, diluted anti-mouse IgG antibody (Santa Cruz Biotechnology, Santa Cruz, CA, USA), and specific proteins were detected using an enhanced chemiluminescence Western blotting analysis system (ECL, Amersham–Pharmacia Biotech, Little Chalfont, UK).

CXCR4 immunostaining. Immunohistochemistry of CXCR4 was performed on 5 μm thick consecutive sections obtained from paraffin-embedded materials. Briefly, the de-paraffinized and hydrated sections were routinely processed with antigen retrieval (0.01 M sodium citrate buffer (pH 6.0) in a microwave oven for 5 min) before incubating for 12 h with anti-CXCR4 monoclonal antibody (R&D Systems, Minneapolis, MN, USA) at 4 °C overnight. This process was performed after inhibition of both endogenous peroxidase activities using 3% H_2O_2 and of non-specific immunoreactivity using 2% normal bovine serum. The sections were incubated with goat anti-mouse IgG biotinylated secondary antibodies (Vectastain ABC Kit, Burlingame, CA, USA) for 1 h at room temperature and thereafter incubated in streptavidin–peroxidase complex for 30 min. The sections were then developed with diaminobenzidine (DAB) as the substrate for 3 min and were counterstained with hematoxylin. In negative controls, an irrelevant antibody replaced the primary antibody. Positive staining was defined as moderate or strong intensity, while negative staining was considered if immunoreactivity was weak or lost.

Migration assay. Cell migration assays were performed in 6.4 mm diameter chambers with 8 μm pore filters (Transwell, 24-well cell cultures; Becton–Dickinson, Bedford, MA). The lower surface of each filter was pre-coated with 50 μg fibronectin (100 μg/mL) and subsequently dried with air blown into a clean ventilator. PC3 and DU145 cells were starved in serum-free RITC 80-7 medium (Kyokuto Pharmaceuticals, Tokyo, Japan) for 24 h. PC3 and DU145 cells were then suspended at 5×10^4 or 20×10^4 cells/mL, respectively, in serum-free RITC 80-7 medium, and then 200 μL of the cell suspension was added to the upper chamber. Various concentrations of SDF-1 (0, 1, 10, 50, or 100 ng/mL) in 600 μL serum-free RITC 80-7 medium were applied in the lower chamber. For neutralization studies, cells pre-treated with 20 μL/mL anti-human CXCR4 monoclonal antibody (44717.111, IgG2B) were incubated for 12 h (for DU145) or 6 h (for PC3) at 37 °C in a humid atmosphere of 5% CO_2. After incubation, the upper surface of the filter was scraped with a cotton swab to remove non-migrating cells, and then the lower surface of the membrane containing the cells that had migrated was stained (Diff-Quick Fixative, Kokusai Shinyaku, Tokyo, Japan). The stained cells were counted under a light microscope (200×). The experiments were performed in triplicate wells.

MTT assay. Effects of SDF-1 on proliferation of prostate cancer cells were analyzed by MTT (Promega, Madison, USA) assay. Cells (1×10^3) of each prostate cancer cell line (PC3 and DU145) were seeded in 96-well plates. After pre-incubation for 1 h with serum-free RITC 80-7 medium, the cells were maintained in RITC 80-7 medium with several concentrations of SDF-1 (0, 1, 10, 50, or 100 ng/mL of SDF-1, or 50 ng/mL) combined with 20 μg/mL anti-human CXCR4 antibody. FBS (5%) was used as a positive control for growth promotion. On days 0, 2, and 4, 15 μg of MTT solution was added and incubated at 37 °C for 4 h. After incubation with MTT solution, solubilization/stop solution of 100 μL was added and incubated at 37 °C for 1 h to completely dissolve the formazan product. Plates were analyzed using an ELISA plate reader (Bio-Rad Laboratories, Hercules, CA) at 570 nm with the reference wavelength set to 630 nm.

Statistical analyses. Results of migration assay and MTT assay were analyzed by Student's *t* test. Relationship between CXCR4 immunostaining and clinicopathological findings was analyzed by χ^2 test or Fisher's exact test. *P* value of less than 0.05 was regarded as statistically significant.

Results

CXCR4 and SDF-1 expression in malignant and normal cultured prostate cells

To confirm the expression of mRNA transcript of CXCR4 and its ligand SDF-1, RT-PCR was performed in LNCaP, PC3, DU145, and PrECs. Total RNA extracted from a pelvic lymph node was used as a positive control. As shown in Fig. 1A, expression of mRNA transcript of CXCR4 was clearly detected in all three PC cell lines, whereas it was not detectable in PrECs. On the other hand, mRNA transcript of SDF-1 was not found in either PC or PrEC lines (Fig. 1A). Similarly, Western blotting clearly showed that CXCR4 expression at protein level was detected in all three prostate cancer cell lines, but not in PrECs (Fig. 1B).

Effect of SDF-1 on chemotaxis of cultured prostate cancer cells

Since expression level of CXCR4 protein in PC3 and DU145 cells was significantly higher than in LNCaP cells (Fig. 1B), chemotactic effect of SDF-1 on PC3 and DU145 cells was analyzed using a migration assay through filters coated with the extracellular matrix protein, fibronectin. SDF-1 at a concentration of 50–100 ng/mL showed a significant increase in migrated PC3 cell counts, and this effect of SDF-1 on PC3 cell migration was significantly inhibited, by a maximum of 39% ($P < 0.05$), by the addition of neutralizing anti-human CXCR4 antibody (Fig. 2A). Likewise, SDF-1 also significantly stimulated the migration ability of DU145 cells with a maximal response observed at 50 ng/mL, and this effect was significantly inhibited, by a maximum of 50% ($P < 0.05$), by neutralizing anti-human CXCR4 antibody (Fig. 2B).

Effect of SDF-1 on growth rate of cultured prostate cancer cells

To investigate whether SDF-1 stimulates the cell growth rate of PC3 and DU145 cells, MTT assay was performed. Contrary to the positive correlation of SDF-1 with chemotactic activity described above, 1–100 ng/mL of SDF-1 treatment did not affect the OD_{570} value in either the PC3 or DU145 cells (Figs. 2C and D). This

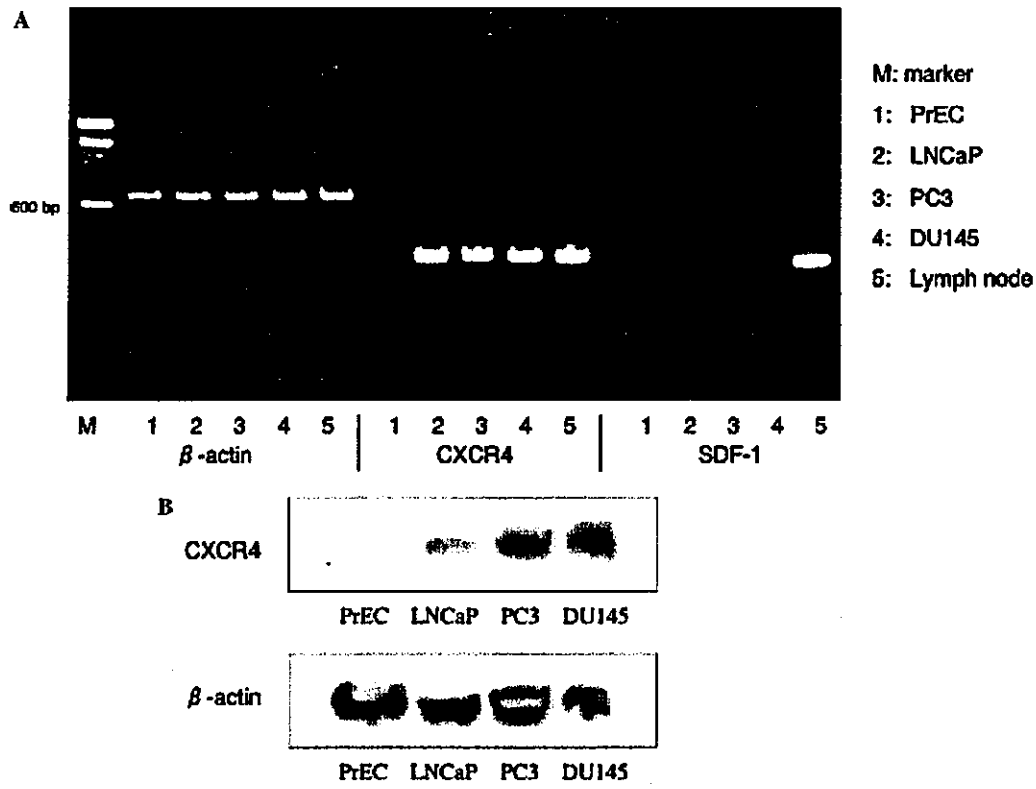

Fig. 1. RT-PCR and Western blotting of CXCR4 and SDF-1 in prostate cancer cell lines and normal PrECs. (A) CXCR4 and SDF-1 mRNA expression as determined by RT-PCR. Lane 1, PrEC; lane 2, LNCaP; lane 3, PC3; lane 4, DU145; and lane 5, pelvic lymph node (as a positive control). SDF-1 expression was not detectable in any of the prostate cancer cell lines. DNA ladder was applied in the left lane. (B) CXCR4 protein expression as determined by Western blotting. CXCR4 expression was detected in all prostate cancer cell lines, but not in normal prostate epithelial cells. β-Actin expression was used as an internal standard.

was not the case in the positive control (5% FBS), in which the OD_{570} value was significantly increased in the presence of 5% FBS ($P < 0.05$). These findings suggest that SDF-1 alone is not sufficient enough to act as a growth factor in prostate cancer cell lines.

CXCR4 protein expression in malignant and non-malignant prostate tissues: relationship between expression of CXCR4 and clinicopathological findings

Typical immunostaining of CXCR4 in non-malignant prostate tissue and PC tissues is shown in Fig. 3. Epithelial cells of non-malignant prostate tissues showed negative CXCR4 immunoreactivity (Fig. 3A); however, in prostate cancer tissues, positive CXCR4 immunoreactivity was observed in 20 of 35 samples (57.1%) (Figs. 3B and C). The relationships between positive CXCR4 immunoreactivity and clinicopathological findings are summarized in Table 1. The positive rate of CXCR4 expression in each group with high PSA value, high clinical T stage, high Gleason sum, positive lymph node metastasis, and positive lung metastasis was higher than in the group of each counterpart, although the difference did not reach statistical significance. There was no significant correlation of CXCR4 expression with PSA value and Gleason sum. Although PSA value is a strong predictor for bone metastasis, logistic regression analysis revealed that positive expression of CXCR4 protein was an independent and superior predictor for bone metastasis to Gleason sum ($P < 0.05$) (Table 1). Patients with positive CXCR4 are 4.5 times more likely to have bone metastasis compared with CXCR4 negative patients. In PC patients with PSA greater than 20 ng/mL, the positive rate of CXCR4 protein was significantly higher in patients with bone metastasis than in those with no bone metastasis ($P = 0.017$).

Discussion

In this study, CXCR4 expression was detected in three PC cell lines of LNCaP, PC3, and DU145 at both the mRNA and protein levels. This was in contrast to normal human prostate epithelial cells, in which no detectable level of CXCR4 expression was found. In addition, we demonstrated that (i) SDF-1 significantly enhanced the migration of PC3 and DU145 cells in a dose-dependent manner and (ii) neutralizing anti-CXCR4 antibody

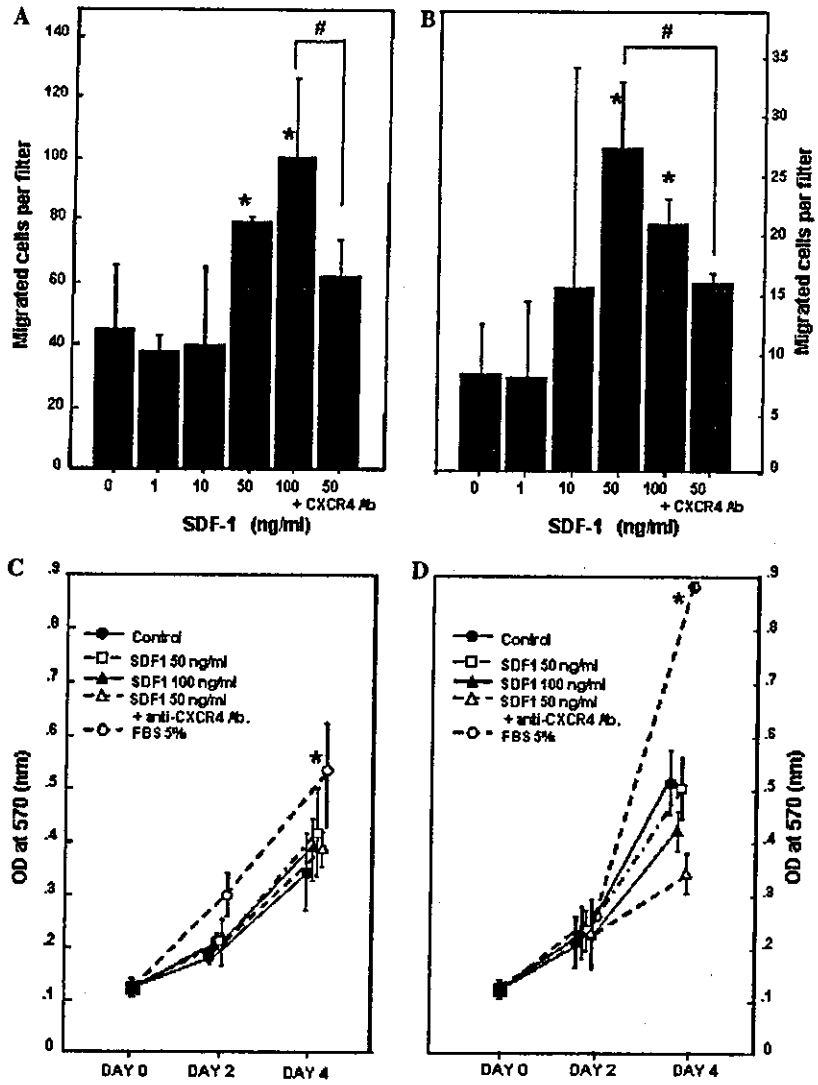

Fig. 2. Migration assay of (A) PC3 and (B) DU145. PC3 or DU145 cells were suspended in the upper chamber, and SDF-1 (0–100 ng/mL) was applied into the lower chamber. Anti-CXCR4 antibody (Ab) was pre-incubated for neutralization study. SDF-1 at 50–100 μg/mL significantly increased the chemotactic ability of PC3 and DU145, and these effects were inhibited by 39% and 50%, respectively, by anti-human CXCR4 neutralizing antibody ($P < 0.05$). Representative results done in triplicate are shown. Data are presented as mean migration of cells per filter. Bars, SD ($n = 3$). *, significant increase over untreated control ($P < 0.05$, Student's t test). #, significant inhibition by anti-CXCR4 Ab ($P < 0.05$, Student's t test). MTT assay of prostate cancer cell lines (C) PC3 and (D) DU145. We assessed 1×10^3 cells of each prostate cell line in serum-free RITC medium with SDF-1 (0–100 ng/mL), SDF-1 plus anti-CXCR4 antibody, or 5% FBS (positive control). SDF-1 did not significantly stimulate the growth rate of both prostate cancer cell lines as compared to the positive control. In comparison with untreated cells, a significant increase was observed only in the cells treated with 5% FBS (*$P < 0.05$). Representative results done in triplicate are shown. Data are presented as means ± SD of OD at wavelength of 570 nm ($n = 3$). Data for 1 and 10 ng/mL SDF-1 are omitted.

inhibited this chemotactic effect of SDF-1. These results indicate that CXCR4 protein, which functions as mediator of SDF-1-involved chemotactic activation, might be de novo expressed during prostatic tumorigenesis. On the other hand, SDF-1 was not expressed in these three prostate cancer cell lines. Therefore, although an autocrine action of SDF-1–CXCR4 ligand–receptor system is supposedly present in neuroblastoma [12], prostate cancer cells might be affected not by endogenous but exogenous SDF-1.

Muller et al. [6] reported that among human organ tissues, SDF-1 mRNA is preferentially expressed in lymph nodes and bone marrow. In bone marrow, osteoblasts, fibroblasts, and endothelial cells constitutively produce SDF-1 [18]. Lymph nodes and bone marrow also represent the most common sites of prostate cancer metastasis. Taking together, our results suggest that PC cells metastasize to specific sites via cell migration mediated by an interaction between SDF-1 and CXCR4 in a paracrine way.

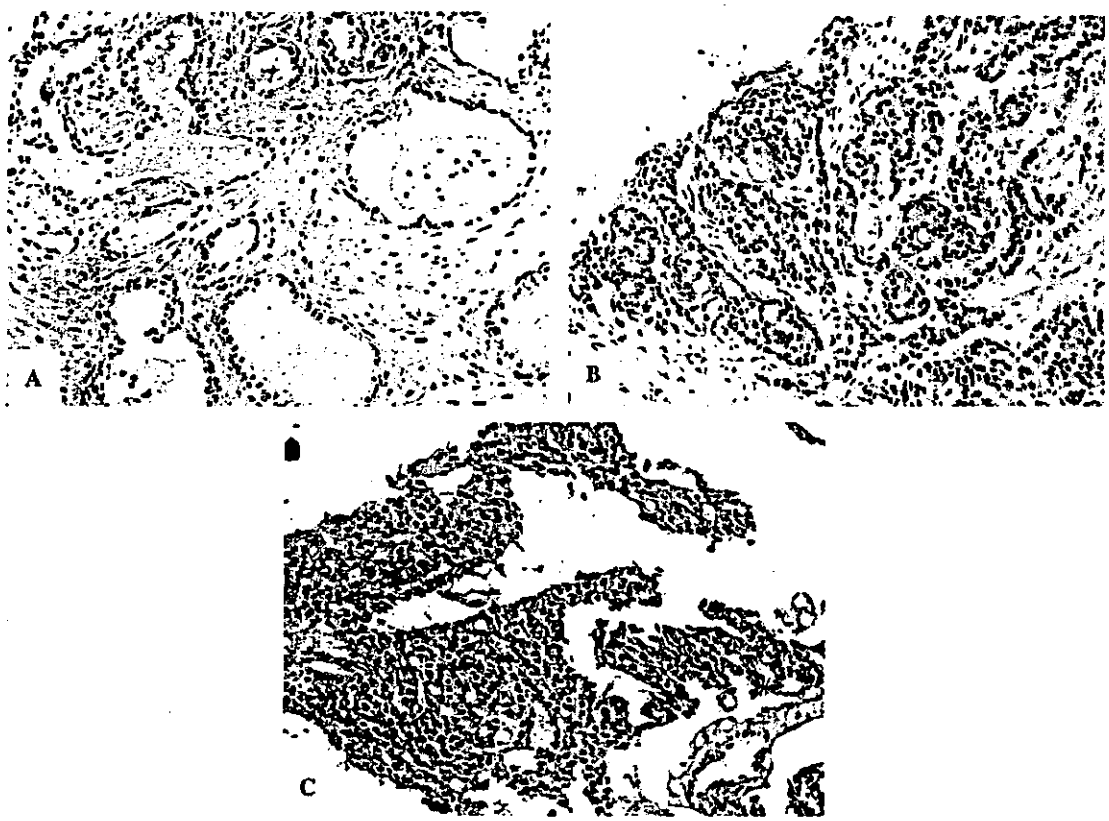

Fig. 3. Immunohistochemical staining for CXCR4 (100×). (A) CXCR4-negative staining. Immunostaining of non-malignant prostate tissue obtained from cystoprostatectomy in a bladder cancer patient is shown. (B) CXCR4-positive staining. Immunostaining of prostate cancer biopsy (PSA 18.6 ng/mL, Gleason grade 3/4 = 7, and linical stage T3N0M0) is shown, where the intensity is moderate. (C) CXCR4-positive staining. Immunostaining of prostate cancer biopsy [PSA 112 ng/mL, Gleason grade 4/5 = 9, and clinical stage T4N1M1 (bone and lung metastasis)] is shown, where the intensity is strong.

With regard to the adhesion of prostate cancer cells to a metastatic site, another process is essential for the establishment of metastasis. A recent investigation revealed that during the adhesion of HSC to endothelial cells or bone marrow stromal cells, rapid but transient activation of integrins by SDF-1 is common, that in turn facilitates the binding of HSC to the cells [3]. This adhesion-promoting effect of SDF-1 mediated by integrin has also been demonstrated in malignant tumors including neuroblastoma [12] and ovarian tumors [9] and thus, a similar adhesion mechanism can be speculated in bone marrow metastasis of prostate cancer [13].

As a final step in metastasis, growth factors available at the metastatic sites enable cancer cells to thrive and proliferate [12,19]. SDF-1 may also help to establish metastasis as a function of growth factors. To confirm this possibility, we performed MTT assay under serum-free conditions in the presence of various concentrations of SDF-1. However, we could not draw any definite conclusion that SDF-1 drives the growth rate of prostate cancer cells. This was consistent with the observation of Taichman et al. [13], where SDF-1 alone does not affect the growth rate of prostate cancer cells. It has been reported that SDF-1 alone does not stimulate the proliferation of early hematopoietic cells but stimulates synergistically with other growth factors [20]. In a study using the lung cancer cell line NCI-H69, SDF-1 did not exert a growth-promoting effect under serum-free conditions but did in the presence of 10% FBS [11]. Thus, SDF-1 alone is not sufficient enough to act as a growth factor and might stimulate prostate cancer cell growth in combination with some other growth factor.

As in the results of the cell culture model described above, we clearly demonstrated that expression of CXCR4 protein was found only in prostate cancer tissues, but not in non-malignant prostate tissues. As shown in Table 1, positive rates of CXCR4 expression were higher in PC patients with worse clinicopathological parameters than in those with better parameters, although the difference was not statistically significant. Logistic regression analysis revealed that positive expression of CXCR4 protein was an independent and superior predictor for bone metastasis compared to Gleason sum ($P < 0.05$). In addition, among PC patients with PSA greater than 20 ng/mL, the positive rate of CXCR4 protein was significantly higher in patients

Table 1
Relationship between expression of CXCR4 and clinicopathological features

Variables	*n*	CXCR4 positive (%)	*P* value
Univariate analysis for CXCR4 expression			
Total	35	20 (57.1)	
PSA (ng/mL)			
4–20	10	5 (50.0)	
20<	25	15 (60.0)	0.71
T category			
T1-2	8	4 (50.0)	
T3-4	27	16 (59.3)	0.70
Cleason sum			
2–6	10	5 (50.0)	
7–10	25	15 (60.0)	0.71
Lymph node metastasis			
Negative	21	10 (47.6)	
Positive	14	10 (71.4)	0.30
Bone metastasis			
Negative	14	5 (35.7)	
Positive	21	15 (71.4)	0.08
Lung metastasis			
Negative	32	17 (53.1)	
Positive	3	3 (100.0)	0.24
Bone metastasis and PSA>20/ng/mL	25		
Negative	4	0 (0.0)	
Positive	21	15 (71.4)	0.017[a]

	SE	Coefficient/SE	χ^2	*P* value	RR
Logistic regression analysis for bone					
CXCR4	0.738	2.038	4.16	0.042	4.5
CXCR4	0.764	1.969	3.876	0.049	4.5
Gleason sum	0.83	1.397	1.952	0.162	3.19
CXCR4	0.975	1.732	2.998	0.083	5.41
PSA	1.231	2.721	7.406	0.007	28.5
Gleason sum	1.038	1.046	1.095	0.295	2.96

[a] Fisher's exact test, SE, standard error; and RR, relative risk.

with bone metastasis than in those with no metastasis. Patients with lung metastasis showed positive immunostaining for CXCR4. Because lymph node metastasis was clinically diagnosed using an imaging study (CT and MRI), this type of metastasis might have been microscopically overlooked. Thus, pathological examination of lymph nodes could have the possibility to improve the correlation between positive CXCR4 immunoreactivity and lymph node metastasis. These findings suggest that CXCR4 expression in PC tissues is closely associated with cancer progression or metastasis and is a useful tool in predicting metastasis in PC patients.

We hypothesize that disruption of the SDF-1–CXCR4 ligand–receptor system could repress metastasis. Our in vitro chemotactic assay demonstrated that anti-CXCR4 antibody blocked SDF-1-induced migration of prostate cancer cells. In a breast cancer metastasis model, Muller et al. [6] reported that administration of an antibody to CXCR4 inhibited metastasis. Similarly, in vivo studies have also shown that a neutralizing antibody to CXCR4 inhibits the homing of human stem cells to the bone marrow in SCID mice [5]. These findings suggest that interaction between SDF-1–CXCR4 ligand–receptor system is involved in the process of PC metastasis by the activation of cancer cell migration.

Acknowledgments

This research was partially supported by the funding from REAP award from Department of Veterans Affairs and Grant-in-Aid for Scientific Research (B) 13470333 and for Encouragement of Young Scientists (B) 14770809 from the Ministry of Education, Science, Sports and culture of Japan.

References

[1] G.L. Nicolson, Paracrine and autocrine growth mechanisms in tumor metastasis to specific sites with particular emphasis on brain and lung metastasis, Cancer Metastasis Rev. 12 (1993) 325–343.
[2] J.M. Wang, X. Deng, W. Gong, S. Su, Chemokines and their role in tumor growth and metastasis, J. Immunol. Methods 220 (1998) 1–17.

[3] A. Peled, O. Kollet, T. Ponomaryov, I. Petit, S. Franitza, V. Grabovsky, M.M. Slav, A. Nagler, O. Lider, R. Alon, D. Zipori, T. Lapidot, The chemokine SDF-1 activates the integrins LFA-1, VLA-4, and VLA-5 on immature human CD34(+) cells: role in transendothelial/stromal migration and engraftment of NOD/SCID mice, Blood 95 (2000) 3289–3296.
[4] D.Y. Jo, S. Rafii, T. Hamada, M.A. Moore, Chemotaxis of primitive hematopoietic cells in response to stromal cell-derived factor-1, J. Clin. Invest. 105 (2000) 101–111.
[5] A. Peled, I. Petit, O. Kollet, M. Magid, T. Ponomaryov, T. Byk, A. Nagler, H. Ben-Hur, A. Many, L. Shultz, O. Lider, R. Alon, D. Zipori, T. Lapidot, Dependence of human stem cell engraftment and repopulation of NOD/SCID mice on CXCR4, Science 283 (1999) 845–848.
[6] A. Muller, B. Homey, H. Soto, N. Ge, D. Catron, M.E. Buchanan, T. McClanahan, E. Murphy, W. Yuan, S.N. Wagner, J.L. Barrera, A. Mohar, E. Verastegui, A. Zlotnik, Involvement of chemokine receptors in breast cancer metastasis, Nature 410 (2001) 50–56.
[7] M.M. Robledo, R.A. Bartolome, N. Longo, J.M. Rodriguez-Frade, M. Mellado, I. Longo, G.N. van Muijen, P. Sanchez-Mateos, J. Teixido, Expression of functional chemokine receptors CXCR3 and CXCR4 on human melanoma cells, J. Biol. Chem. 276 (2001) 45098–45105.
[8] A.S. Payne, L.A. Cornelius, The role of chemokines in melanoma tumor growth and metastasis, J. Invest. Dermatol. 118 (2002) 915–922.
[9] C.J. Scotton, J.L. Wilson, K. Scott, G. Stamp, G.D. Wilbanks, S. Fricker, G. Bridger, F.R. Balkwill, Multiple actions of the chemokine CXCL12 on epithelial tumor cells in human ovarian cancer, Cancer Res. 62 (2002) 5930–5938.
[10] T. Koshiba, R. Hosotani, Y. Miyamoto, J. Ida, S. Tsuji, S. Nakajima, M. Kawaguchi, H. Kobayashi, R. Doi, T. Hori, N. Fujii, M. Imamura, Expression of stromal cell-derived factor 1 and CXCR4 ligand receptor system in pancreatic cancer: a possible role for tumor progression, Clin. Cancer Res. 6 (2000) 3530–3535.
[11] T. Kijima, G. Maulik, P.C. Ma, E.V. Tibaldi, R.E. Turner, B. Rollins, M. Sattler, B.E. Johnson, R. Salgia, Regulation of cellular proliferation, cytoskeletal function, and signal transduction through CXCR4 and c-Kit in small cell lung cancer cells, Cancer Res. 62 (2002) 6304–6311.
[12] H. Geminder, O. Sagi-Assif, L. Goldberg, T. Meshel, G. Rechavi, I.P. Witz, A. Ben-Baruch, A possible role for CXCR4 and its ligand, the CXC chemokine stromal cell-derived factor-1, in the development of bone marrow metastases in neuroblastoma, J. Immunol. 167 (2001) 4747–4757.
[13] R.S. Taichman, C. Cooper, E.T. Keller, K.J. Pienta, N.S. Taichman, L.K. McCauley, Use of the stromal cell-derived factor-1/CXCR4 pathway in prostate cancer metastasis to bone, Cancer Res. 62 (2002) 1832–1837.
[14] D.F. Gleason, Histologic grading of prostate cancer: a perspective, Human Pathol. 23 (1992) 273–279.
[15] L.H. Sobin, I.D. Fleming, TNM Classification of Malignant Tumors, fifth edition (1997). Union Internationale Contre le Cancer and the American Joint Committee on Cancer, Cancer 80 (1997) 1803–1804.
[16] M. D'Apuzzo, A. Rolink, M. Loetscher, J.A. Hoxie, I. Clark-Lewis, F. Melchers, M. Baggiolini, B. Moser, The chemokine SDF-1, stromal cell-derived factor 1, attracts early stage B cell precursors via the chemokine receptor CXCR4, Eur. J. Immunol. 27 (1997) 1788–1793.
[17] C.C. Bleul, R.C. Fuhlbrigge, J.M. Casasnovas, A. Aiuti, T.A. Springer, A highly efficacious lymphocyte chemoattractant, stromal cell-derived factor 1 (SDF-1), J. Exp. Med. 184 (1996) 1101–1109.
[18] T. Ponomaryov, A. Peled, I. Petit, R.S. Taichman, L. Habler, J. Sandbank, F. Arenzana-Seisdedos, A. Magerus, A. Caruz, N. Fujii, A. Nagler, M. Lahav, M. Szyper-Kravitz, D. Zipori, T. Lapidot, Induction of the chemokine stromal-derived factor-1 following DNA damage improves human stem cell function, J. Clin. Invest. 106 (2000) 1331–1339.
[19] R. Radinsky, I.J. Fidler, Regulation of tumor cell growth at organ-specific metastases, In Vivo 6 (1992) 325–331.
[20] S.K. Gupta, K. Pillarisetti, Cutting edge: CXCR4-Lo: molecular cloning and functional expression of a novel human CXCR4 splice variant, J. Immunol. 163 (1999) 2368–2372.

Molecular Cell, Vol. 14, 363–374, May 7, 2004, Copyright ©2004 by Cell Press

Structural Basis for Octameric Ring Formation and DNA Interaction of the Human Homologous-Pairing Protein Dmc1

Takashi Kinebuchi,[1] Wataru Kagawa,[1] Rima Enomoto,[1] Kozo Tanaka,[2] Kiyoshi Miyagawa,[2] Takehiko Shibata,[3] Hitoshi Kurumizaka,[1,4,6,*] and Shigeyuki Yokoyama[1,4,5,7,*]
[1]Protein Research Group
RIKEN Genomic Sciences Center
1-7-22 Suehiro-cho, Tsurumi
Yokohama 230-0045
[2]Department of Molecular Pathology
Research Institute for Radiation Biology and Medicine
Hiroshima University
1-2-3 Kasumi, Minami-ku
Hiroshima 734-8553
[3]Cellular and Molecular Biology Laboratory
RIKEN
2-1 Hirosawa, Wako-shi
Saitama 351-0198
[4]Cellular Signaling Laboratory
RIKEN Harima Institute at SPring-8
1-1-1 Kohto, Mikazuki-cho, Sayo
Hyogo 679-5148
[5]Structurome Research Group
RIKEN Harima Institute at SPring-8
1-1-1 Kohto, Mikazuki-cho, Sayo
Hyogo 679-5148
[6]Waseda University School of Science and Engineering
3-4-1 Okubo, Shinjuku-ku
Tokyo 169-8555
[7]Department of Biophysics and Biochemistry
Graduate School of Science
University of Tokyo
7-3-1 Hongo, Bunkyo-ku
Tokyo 113-0033
Japan

Summary

The human Dmc1 protein, a RecA/Rad51 homolog, is a meiosis-specific DNA recombinase that catalyzes homologous pairing. RecA and Rad51 form helical filaments, while Dmc1 forms an octameric ring. In the present study, we crystallized the full-length human Dmc1 protein and solved the structure of the Dmc1 octameric ring. The monomeric structure of the Dmc1 protein closely resembled those of the human and archaeal Rad51 proteins. In addition to the polymerization motif that was previously identified in the Rad51 proteins, we found another hydrogen bonding interaction at the polymer interface, which could explain why Dmc1 forms stable octameric rings instead of helical filaments. Mutagenesis studies identified the inner and outer basic patches that are important for homologous pairing. The inner patch binds both single-stranded and double-stranded DNAs, while the outer one binds single-stranded DNA. Based on these results, we propose a model for the interaction of the Dmc1 rings with DNA.

*Correspondence: kurumizaka@waseda.jp (H.K.); yokoyama@biochem.s.u-tokyo.ac.jp (S.Y.)

Introduction

Homologous recombination is involved in many biologically important processes. In mitosis, double-stranded DNA breaks, which are frequently induced by ionizing radiation and replication errors, are repaired through the homologous-recombinational repair pathway (Symington, 2003). In meiosis, a physical connection between homologous chromosomes is established by homologous recombination (meiotic recombination) to ensure proper chromosome segregation (Kleckner, 1996; Roeder, 1997). Meiotic recombination also contributes to genetic variation, by creating new linkages between genes or parts of genes.

In bacterial homologous recombination, the RecA protein is a key enzyme that catalyzes the homology search and exchange between two DNA molecules ("homologous pairing"). The *Escherichia coli* RecA protein has been the most intensively studied homologous-pairing enzyme. The crystal structure of *E. coli* RecA revealed an ATPase domain structure organized into a helical filament with six monomers per turn (Story et al., 1992). Studies have shown that during the homologous-pairing reaction, RecA forms a ternary complex with ssDNA and dsDNA (Tsang et al., 1985), which draws the two DNA molecules close together and thereby allows the efficient search and exchange. The RecA•ssDNA•dsDNA ternary complex forms a nucleoprotein filament (Stasiak et al., 1984), and the RecA-bound ssDNA is stretched 1.5 times longer than the B form DNA (Stasiak et al., 1981; Stasiak and DiCapua, 1982; Nishinaka et al., 1997).

The Rad51 protein, a eukaryotic homolog of RecA, is considered to be a central player in the homologous recombination pathway. The yeast and human Rad51 proteins form similar nucleoprotein filaments, as compared with those of the bacterial RecA protein (Ogawa et al., 1993; Benson et al., 1994). This suggests that the key structural properties of nucleoprotein filaments, depending on both the protein geometry and the DNA structure (Yang et al., 2001a), have been conserved over large evolutionary distances. The crystal structure of the human Rad51 ATPase domain, covalently linked to the BRC repeat 4 of the BRCA2 protein, revealed that the overall topology of the ATP domain closely resembled that of the RecA protein (Pellegrini et al., 2002).

The archaeal homolog of RecA/Rad51 is known as the RadA protein. RadA is capable of catalyzing an in vitro strand exchange reaction in a similar manner to that of Rad51 (Seitz et al., 1998; Komori et al., 2000; Spies et al., 2000; Miyata et al., 2000). Recent studies have shown that the *Sulfolobus solfataricus* RadA protein exists in two different oligomeric states, an octameric ring and a helical filament, and that both states can bind to DNA (Yang et al., 2001b). The structure of *Pyrococcus furiosus* RadA (PfRad51) (Shin et al., 2003) was determined to be a heptameric ring structure. How-

Table 1. Crystallographic Statistics

Data Collection	
Wave length	0.9821 Å
Resolution (Å)	50.0-3.2
Reflections (measured/unique)	95,595/14,093
Completeness (%; overall/outer shell)	97.8/97.2
R_{sym} (%; overall/outer shell)	7.3/39.6
$I/\sigma(I)$	18.8/2.62
Refinement	
Resolution (Å)	20.0-3.2
Residues	478
Atoms	3,767
Average B value (main/side chain)	81.9/90.5
[1]R-factor (overall/outer shell)	29.4/45.1
[2]R_{free} (overall/outer shell)	34.6/45.1
Bond lengths (Å)	0.009
R.m.s.d. Bond angles (°)	1.41

[1]R-factor = $\Sigma_{hkl}|F_{obs} - F_{calc}|/\Sigma_{hkl}|F_{obs}|$
[2]$R_{free} = \Sigma_{hkl\in T}|F_{obs} - F_{calc}|/\Sigma_{hkl\in T}|F_{obs}|$, where the test set T includes 10% of the data.

ever, electron microscopic studies have shown that PfRad51-DNA complexes form nucleoprotein filaments, suggesting that the recombination-active form of PfRad51 is a helical filament (Komori et al., 2000).

Eukaryotes carry the Dmc1 protein, a meiotic homolog of the Rad51 protein, with which it shares extensive sequence similarity (Bishop et al., 1992). Dmc1 was first discovered in yeast, and subsequently has been found in many mammals (Habu et al., 1996). The knockout of *DMC1* in the mouse causes asynapsis and sterility (Pittman et al., 1998; Yoshida et al., 1998), suggesting the importance of Dmc1 in meiotic recombination. Previous biochemical experiments revealed that Dmc1 promotes homologous pairing as well as strand exchange between single-stranded and double-stranded DNA (Li et al., 1997; Masson et al., 1999; Hong et al., 2001; Masson and West, 2001). Since Dmc1 exhibits extensive sequence similarity to Rad51, the Dmc1 protein was expected to catalyze homologous pairing by a RecA/Rad51-like mechanism. This mechanism includes the formation of a nucleoprotein filament and the subsequent search for homologous sequences between the two DNA molecules in the ternary complex. Surprisingly, however, several recent electron microscopic studies failed to detect helical filament formation by Dmc1 (Masson et al., 1999; Passy et al., 1999). Instead, these studies showed that Dmc1 forms an octameric ring structure. These rings were found to form complexes composed of stacked rings on DNA.

In the present study, the octameric ring structure of the Dmc1 protein was determined at 3.2 Å resolution. We have identified hydrogen bonds at the monomer-monomer interfaces that are essential for the octamer formation. These hydrogen bonds are probably absent from Rad51. In addition, alanine-scanning mutagenesis has revealed essential ssDNA and dsDNA binding sites.

Results and Discussion

The Dmc1 Octameric Ring Structure

The full-length human Dmc1 protein was successfully crystallized, and the structure ($Dmc1_{83-340}$) was solved by the molecular replacement method, using the human Rad51 ATPase domain structure as a guide (Table 1). This was indicative of the highly conserved monomeric structures between Dmc1 and Rad51. In fact, the ATPase domain of Dmc1, solved at 3.2 Å resolution (see Supplemental Figure S1 at http://www.molecule.org/cgi/content/full/14/3/363/DC1), was nearly identical to those of the human and *Pyrococcus furiosus* Rad51 proteins (human Rad51 (Pellegrini et al., 2002), RMSD of 0.645 Å over 178 Cα atoms; archaeal PfRad51 (Shin et al., 2003), RMSD of 0.73 Å over 177 Cα atoms), and closely resembled that of *E. coli* RecA protein (Story et al., 1992) (RMSD of 1.77 Å over 160 Cα atoms).

The crystal structure of Dmc1 revealed a highly symmetrical octameric ring, with a 4-fold crystallographic symmetry axis running through the center of the ring structure (Figures 1A and 1B). The two monomers present in the asymmetric unit had an RMSD of 0.012 Å. In particular, the structures of the residues at the monomer-monomer interface, including those related by non-crystallographic symmetry and crystallographic symmetry, were near identical. The outer diameter of the Dmc1 ring was 130 Å, and the inner diameter of the ring was 27 Å. These dimensions are consistent with those estimated from the electron micrographs of the Dmc1 protein (Passy et al., 1999). In the presence of DNA, the stacked Dmc1 rings were bipolar in appearance (Passy et al., 1999). Interestingly, in the crystals used for our structural determination, the two stacked Dmc1 rings were bipolar (Figure 1C), and formed a repeating unit. This dimer of Dmc1 octamers (double ring) observed in the crystals may closely resemble the stacked Dmc1 rings bound to DNA, as observed by electron microscopy (Passy et al., 1999). In the absence of DNA, however, Dmc1 exists as single, octameric rings in solution, as revealed by analytical ultracentrifugation (Figure 1D).

About 30% of the Dmc1 protein (the N-terminal region, $Dmc1_{1-82}$, and the putative DNA binding region (Loop 2), $Dmc1_{271-289}$) was uninterpretable from the calculated electron density maps, suggesting that these regions are either highly flexible or have multiple conformations. To confirm that these regions were not proteolyzed during crystallization, the Dmc1 crystals were subjected to SDS-PAGE. No degradation products of Dmc1 were observed (data not shown), indicating that $Dmc1_{1-82}$ and $Dmc1_{271-289}$ were disordered in the crystals. The PfRad51 structure also exhibited high flexibility in these regions (Shin et al., 2003). In the Dmc1 structure, the N-terminal domain is predicted to be located near the monomer-monomer interface, and thus it may have a role in octamer ring stability. Interestingly, Passy et al. observed a small fraction of heptamers in Dmc1 preparations containing a low percentage of a cleavage product, which closely corresponded to the Dmc1 protein lacking the N-terminal domain. By contrast, only octamers were observed in a different Dmc1 preparation that was free of degradation (Passy et al., 1999). The present structure supports the view that the N-terminal domain contributes a steric bulk to force Dmc1 to form octamers instead of heptamers. In addition, the N-terminal domain of the human Rad51 protein has been shown to directly interact with DNA (Aihara et al., 1998), suggesting that the N-terminal domain of Dmc1 may also function in DNA binding. These observations indicate multiple and essential roles of the N-terminal domain of Dmc1.

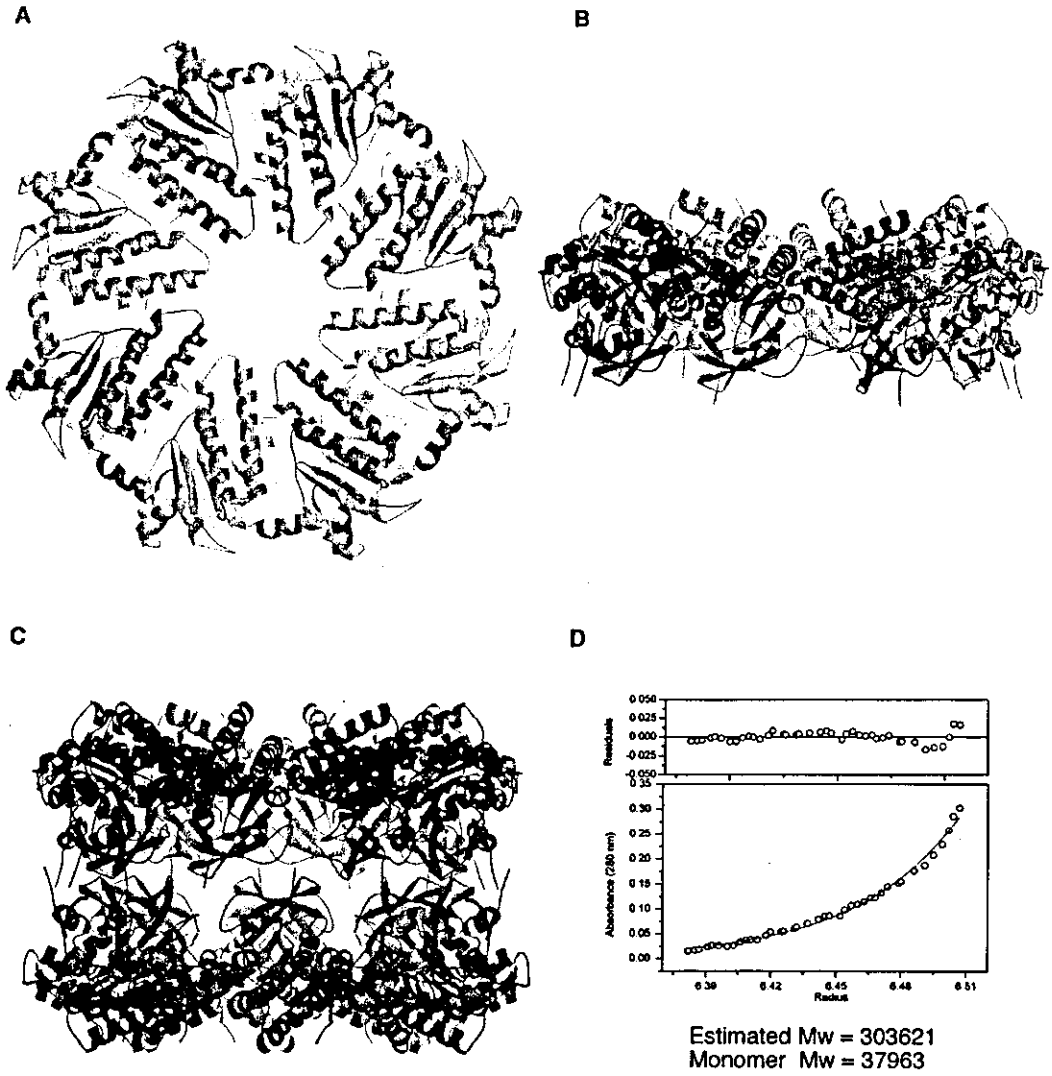

Figure 1. The Octameric Ring Structure of Dmc1

(A) Ribbon diagram of the octameric ring structure of Dmc1, viewed down the central channel from the top of the ring. Each monomer is colored differently, and the ring has a 4-fold rotational symmetry axis running down the center. (B) A view from the side of the ring. (C) Double ring structure of Dmc1. (D) Sedimentation equilibrium analysis of the Dmc1 protein. For the molecular weight analysis, the data were fit to an ideal, single component model.

Structural Determinants for the Octameric Ring

A previous structural study on the ATPase domain of the human Rad51 protein covalently linked to the BRC 4 repeat of the BRCA2 protein revealed a putative polymerization motif (FxxA) within Rad51 (Pellegrini et al., 2002). The same motif was also found in the PfRad51 structure, which was organized in a heptameric ring structure (Shin et al., 2003). The polymerization motif participates in two interactions. One involves a phenylalanine residue (corresponding to Phe85 of Dmc1) that displays a "ball-and-socket" hydrophobic interaction with the residues of the adjacent monomer. The other interaction includes hydrogen bonding between β0 and β3 of the adjacent monomer. These two interactions were well conserved in the Dmc1 octameric ring structure (Figures 2A and 2B), suggesting the widespread conservation of this motif. Interestingly, homologs of Dmc1 have been shown to form ring structures with different numbers of subunits (Heuser and Griffith, 1989; Yu and Egelman, 1997; Yang et al., 2001b). Regardless of the differences in oligomerization states, the atomic resolution structures of PfRad51 and Dmc1 indicate that these proteins utilize the same motif to form ring structures. While the role of this motif in the helical filament form of Rad51 awaits its detailed structure, the broad conservation of the motif suggests its involvement in helical filaments as well.

In the present Dmc1 structure, we found that the Glu258 residue forms tripartite hydrogen bonds with Asn163, Arg192, and Tyr194 of the adjacent monomer (Figures 2A and 2C). The Glu258 residue is well conserved among the Dmc1 homologs, while all of the

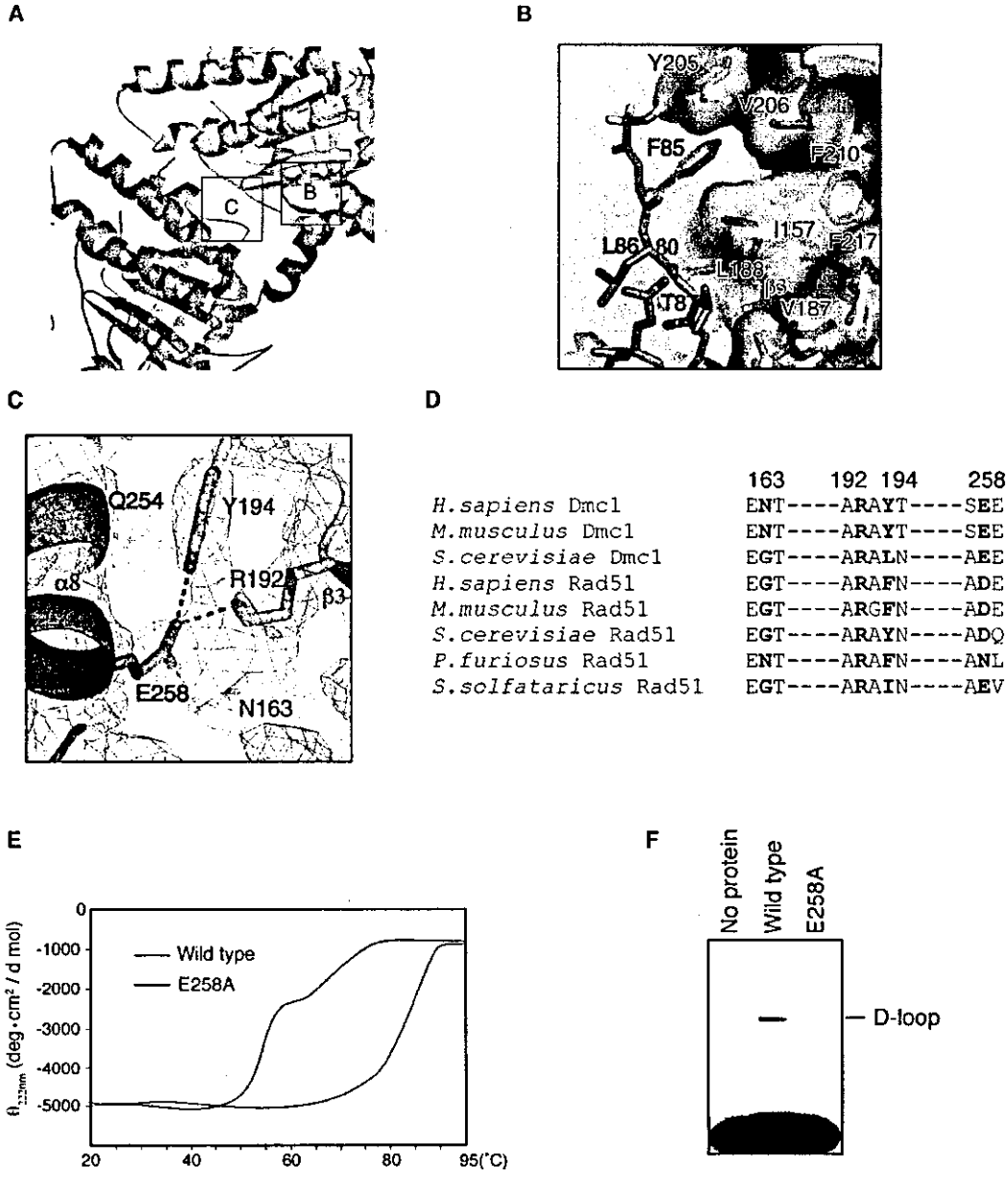

Figure 2. The Monomer-Monomer Interface of Dmc1

(A) A close-up view of the interface. (B) The polymerization motif (Pellegrini et al., 2002; Shin et al., 2003) is formed by an intersubunit β sheet (between β0, colored green, and β3, colored yellow). The hydrogen bonding between the monomers is shown as pink dotted lines. (C) Additional hydrogen bonds at the interface stabilize the octameric ring formation. The hydrogen bonds between monomers are shown as pink dotted lines. Green and yellow colors indicate each monomer. The $2|F_o|-|F_c|$ electron density map, contoured at 1.0 σ, is shown in blue. (D) Sequence alignment of the residues included in the hydrogen bonds of Dmc1, from human, mouse, and yeast, and those of Rad51, from human, mouse, and archaea. (E) Temperature dependence of the CD effect at 222 nm, as a function of temperature for the wild-type Dmc1 (blue) and E258A (red). (F) D loop formation by Dmc1. The Dmc1 protein and E258A mutants (5 μM) were preincubated with a 50-mer ssDNA (1 μM) for 5 min, followed by the addition of a superhelical dsDNA (10 μM, 3,218 bp) to initiate the reaction. Assays were analyzed by 1% agarose gel electrophoresis.

eukaryotic Rad51 homologs have an aspartic acid residue at this position (Figure 2D). Since the aspartic acid residue is shorter by one carbon in its side chain, as compared with that of the glutamic acid residue, Rad51 may be incapable of forming hydrogen bonds in the ring or helical filament form. Actually, the PfRad51 heptameric ring lacks this additional hydrogen-bonding interface (Shin et al., 2003).

Another notable difference at the interface is that Rad51 proteins have a hydrophobic residue corresponding to the Gln254 residue of Dmc1, while all Dmc1 proteins have a hydrophilic residue at this position (see

Supplemental Figure S1 at http://www.molecule.org/cgi/content/full/14/3/363/DC1). In the heptameric storage form of PfRad51, the His269 (corresponding to Gln254 of Dmc1) residue is stacked with Phe206 (corresponding to Tyr194 of Dmc1), thus creating a slippery surface for the PfRad51 to transition into a filament (Shin et al., 2003). This contrasts with Dmc1, in which Tyr194 points away from Gln254 and participates in the tripartite hydrogen bonding with Glu258 (Figure 2C). Therefore, these structural features at the interface of Dmc1, which seem to be distinct from those of Rad51, stabilize the octameric ring.

We then prepared a mutant with an alanine in place of Glu258 (E258A), and analyzed the effect of the mutation on the stability of the octameric ring by circular dichroism (CD) spectroscopy. CD spectra were collected for the E258A mutant and the wild-type protein at 222 nm, while the temperature was gradually raised from 20 to 95°C (Figure 2E). The wild-type protein showed a sharp increase in ellipticity around 82°C, indicating that the transition from the octameric state to the denatured monomeric state occurred cooperatively. In contrast, the E258A mutant exhibited biphasic melting, at 54°C and 70°C. The first and second phases may correspond to the melting of the quaternary and tertiary structures, respectively. These results indicate that the Glu258 residue is important for the stabilization of the Dmc1 octamer. Electron microscopy of the E258A mutant revealed some ring structures, but structurally undefined aggregates were also quite prevalent (data not shown). The wild-type Dmc1 proteins were observed predominantly in the octameric ring structure (Passy et al., 1999; Figure 1D). Aggregation of the E258A mutant was also suggested by analytical ultracentrifugation and gel filtration analyses (data not shown).

To examine the functional effects of this mutation, the homologous-pairing activity of the E258A mutant was compared to that of the wild-type protein. The human Dmc1 protein catalyzes strand assimilation between ssDNA and supercoiled dsDNA (Li et al., 1997; Figure 2F). In contrast, the E258A mutant was completely defective in homologous pairing (Figure 2F). These results suggest that Glu258, an interface residue essential for the stabilization of the octamer ring, plays a critical role in homologous pairing, thus supporting the idea that the octameric ring is the functional form of Dmc1. Interestingly, Dmc1 and Rad51 exhibit clear differences in their quaternary structures, although they are highly homologous to each other and are both capable of promoting homologous pairing in vitro.

The DNA Binding Site

The surface potential analysis of the Dmc1 octamer revealed two basic patches (per monomer) on the bottom side of the ring, which are potential DNA binding sites (Figures 3A and 3B). To locate the precise ssDNA and dsDNA binding sites, we performed an alanine-scanning mutagenesis of the basic and aromatic residues located on these basic patches (Arg230, Phe233, Arg236, Arg242, Arg304, Lys305, Arg307, and Arg311) (Figures 3D and 3E). The Arg230, Phe233, Arg236, and Arg242 residues were located near the central channel of the ring structure (inner basic patch), and Arg304, Lys305, Arg307, and Arg311 were located near the perimeter of the ring structure (outer basic patch). These residues are conserved among the Dmc1 and Rad51 proteins. Prior to examining the DNA binding activities of the purified mutants, electron microscopy was employed to confirm that each mutant was able to form ring structures, with no discernable differences as compared with those formed by the wild-type protein (data not shown).

As shown in Figure 4A, ssDNA binding was affected significantly by the mutations on the inner basic patch (Arg230, Phe233, Arg236, and Arg242), and by one mutation on the outer basic patch (Arg311). The other mutations on the outer basic patch (Arg304, Lys305, and Arg307) had little or no effect on the ssDNA binding activity of Dmc1 (Figure 4A). Previous mutagenesis studies of the PfRad51 protein did not define any role for the residue corresponding to the Dmc1 Arg236 residue in the ssDNA-dependent ATPase activity (Shin et al., 2003). Interestingly, the mutation of Arg236 to alanine caused a drastic reduction in the ssDNA-dependent ATPase activity (data not shown), suggesting that the ATP binding regions of the Rad51 and Dmc1 monomers could have different geometric orientations when bound to ssDNA.

The mutant Dmc1 proteins were then tested for their dsDNA binding abilities, using linear dsDNA as the substrate. As shown in Figure 4B, mutations on the inner basic patch (Arg230, Arg236, and Arg242) caused significant defects in the dsDNA binding. In contrast, mutations on the outer basic patch (Arg304, Lys305, Arg307, and Arg311) had little or no effect on the dsDNA binding (Figure 4B).

The inner basic patch includes the Loop I region, which was identified as an essential site for ssDNA and dsDNA binding in RecA (Story et al., 1992). In the Dmc1 protein, this region was essential for both ssDNA and dsDNA binding (Figures 4A and 4B). In particular, the Phe233 residue was quite important for ssDNA binding, and may undergo hydrophobic stacking with the bases of the ssDNA molecule. In contrast to the inner basic patch, the basic residues on the outer basic patch were either specifically important for ssDNA binding (Arg311) or not directly involved in DNA binding (Arg304, Lys305, Arg307). Phe233, on the inner basic patch, and Arg311, on the outer basic patch, could have roles in guiding the ssDNA to the inner basic patch, which may be the catalytic center for homologous pairing.

Ternary Complex Formation

The human Dmc1 protein catalyzes homologous pairing between ssDNA and supercoiled dsDNA in an ATP-dependent manner (Li et al., 1997; Figure 4C). Furthermore, D loop formation is inhibited in the presence of ATP-γ-S (Li et al., 1997), while interestingly, the D loop formation of the yeast Dmc1 protein is enhanced in the presence of AMP-PNP (Hong et al., 2001). We have confirmed the homologous-pairing activity of the human Dmc1 protein (~10% of the dsDNA substrate was incorporated into the product, which corresponded to ~30% of the activity of *E. coli* RecA). In addition, product formation was enhanced 2- to 3-fold by the addition of AMP-PNP (Figure 4C).

Contrary to our expectations, the mutants that were

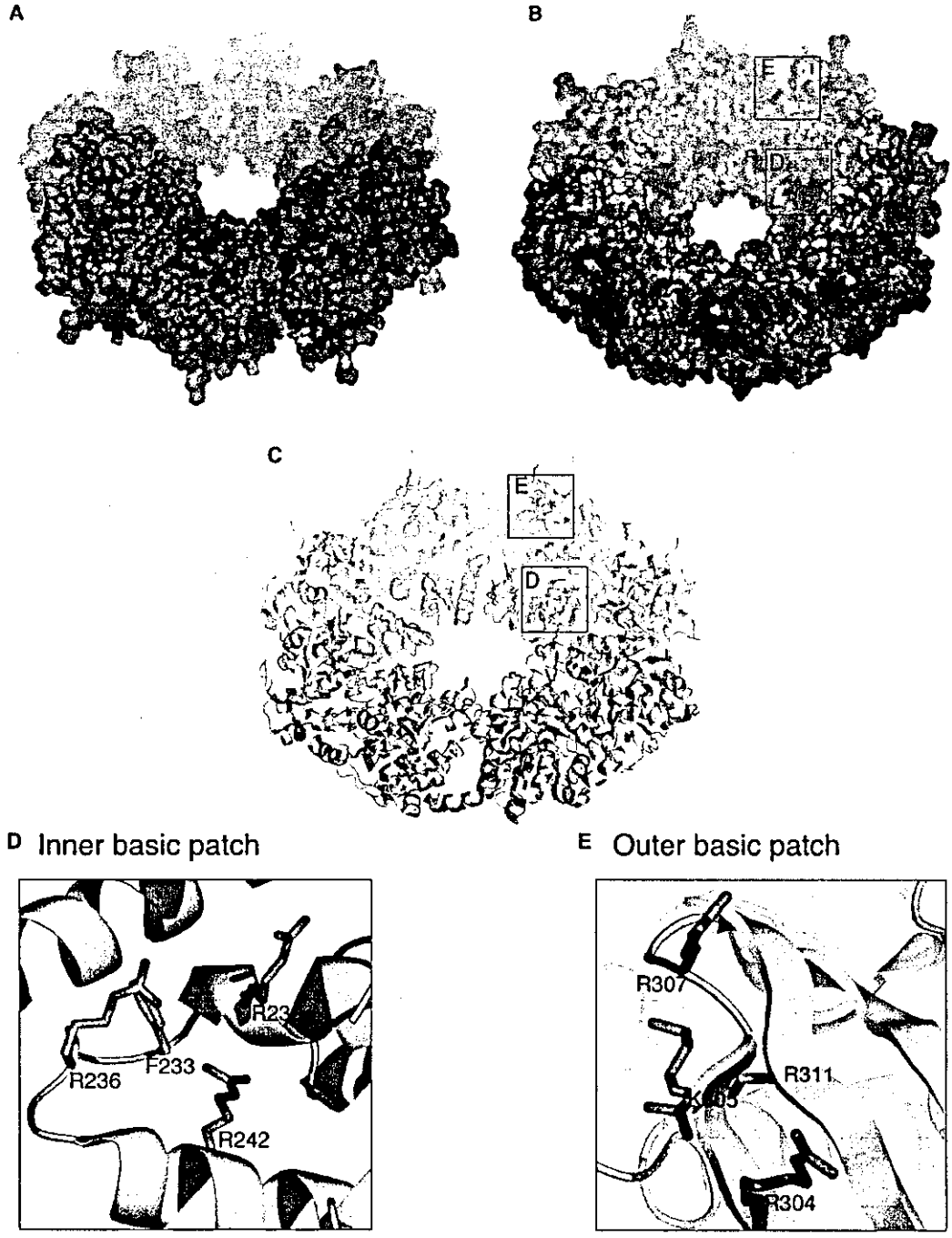

Figure 3. Surface Views of the Dmc1 Octamer and the Locations of the Residues Subjected to Alanine-Scanning Mutagenesis

Electrostatic surface potential of Dmc1 viewed from the top (A) and bottom (B). Surfaces are colored according to the local electrostatic potential, from $-10\ k_BT^{-1}$ (red) to $+10\ k_BT^{-1}$ (blue). Electrostatic surface potentials were calculated using the GROMACS (Berendsen et al., 1995; Lindahl et al., 2001) and MEAD (Bashford and Gerwert, 1992) programs. (C) Ribbon model of the Dmc1 octamer, viewed from the same angle as in (B). The side chains of the amino acid residues targeted for mutagenesis are depicted. These residues are located on the two basic patches shown in (B). The outer basic patch residues are colored magenta, while the inner basic patch residues are cyan. Close-up views of the boxed portions are shown in (D) and (E).

proficient in both ssDNA and dsDNA binding (Arg304, Lys305, Arg307) were completely defective in homologous pairing (Figure 4D). We then examined whether Dmc1 and its mutants formed the intermediate complex (ternary complex) during the homologous-pairing reaction. When ^{32}P-labeled ssDNA and superhelical dsDNA were sequentially added to the reaction mixture containing Dmc1, which was then fixed with glutaraldehyde

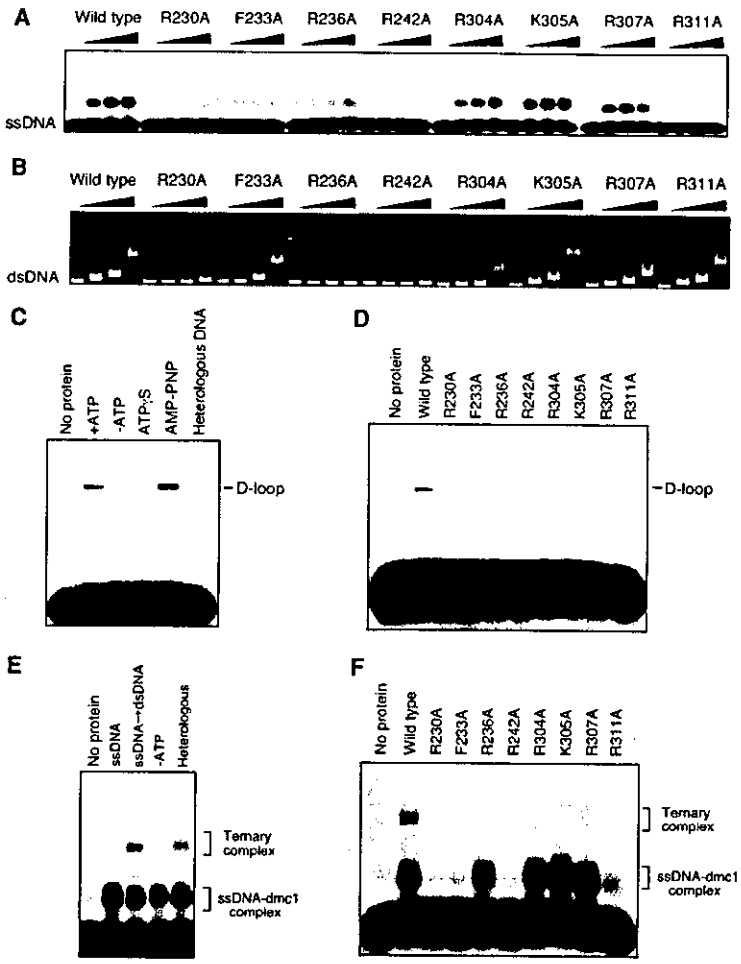

Figure 4. DNA Binding, Ternary Complex Formation, and D Loop Formation by Dmc1

All assays were analyzed by 1% agarose gel electrophoresis. (A) ssDNA binding by Dmc1 and its point mutants was analyzed by incubating 2.5, 5, and 10 μM concentrations of the proteins with a 50-mer ssDNA (1 μM). (B) dsDNA binding by Dmc1 and its point mutants was analyzed by incubating 0.5, 1, and 5 μM concentrations of the proteins with a linear φX174 plasmid DNA (10 μM, 5,386 bp). D loop assay of Dmc1 (C) and its point mutants (D). The Dmc1 protein and its point mutants (5 μM) were preincubated with a 50-mer ssDNA (1 μM) for 5 min, followed by the addition of a superhelical dsDNA (10 μM, 3,218 bp) to initiate the reaction. Ternary complex formation by Dmc1 (E) and its point mutants (F). Dmc1 (5 μM) was preincubated with a 50-mer ssDNA (1 μM) for 5 min, followed by the addition of a superhelical dsDNA (10 μM, 3,218 bp) to initiate the reaction. For the ternary complex formation by the Dmc1 point mutants, the same procedure was followed, using 5 μM of each protein.

and fractionated by agarose gel electrophoresis, ternary complexes were observed. As shown in Figure 4E, when ssDNA was added before dsDNA, the ternary complexes were formed, which migrated more slowly than the Dmc1-ssDNA complex. The formation of ternary complexes was ATP dependent and homology independent (Figure 4E). The homology-independent reaction indicates that the base pairing between the ssDNA and dsDNA molecules is not necessarily required in the ternary complex. This activity is reminiscent of the homology search mechanism of the RecA protein, which is known to actively search for homologous sequences between the two recombining DNA molecules within the ternary complex containing both ssDNA and dsDNA molecules. Interestingly, while Dmc1 forms an octameric ring structure and RecA forms a helical filament, the Dmc1 protein may also have a homology search mechanism similar to that of the RecA protein.

As shown in Figure 4F, all of the mutants had drastic reductions in their abilities to form ternary complexes, as compared with the wild-type. Notably, the R304A, K305A, and R307A mutants had ssDNA and dsDNA binding activities almost equivalent to those of the wild-type Dmc1 protein. These mutants were proficient in hydrolyzing ATP, as compared with the wild-type Dmc1 protein (data not shown). Despite their similar DNA binding and ATPase activities, the ternary complex formation was drastically reduced by these mutations. Therefore, Arg304, Lys305, and Arg307 in the outer basic patch may play essential roles in ternary complex formation. Since these residues are located near the interface of the stacked rings (Figure 5B), they could promote the formation of a functional Dmc1 double ring on DNA.

Model for Ternary Complex Formation by Dmc1

The hypothesis in which the Dmc1 molecule primarily functions as octameric rings is supported by the interface we found that involves the Glu258 residue. However, we cannot exclude the possibility that Dmc1 may form helical filaments, because Rad51 and RecA form both rings and helical filaments and Dmc1 exhibits strong sequence similarity to these proteins (Ogawa et al., 1993; Baumann et al., 1997; Yu and Egelman, 1997; Yang et al., 2001b). Nevertheless, only rings have been observed in electron microscopic analyses of Dmc1 (Masson et al., 1999; Passy et al., 1999). Furthermore, the ssDNA-dependent ATPase activities of the Dmc1 R236A mutant and its counterpart in PfRad51 were different (Shin et al., 2003), suggesting structural differences between Dmc1 and the helical filament-forming PfRad51. These experimental results support the importance of the Dmc1 octamer function in recombination.

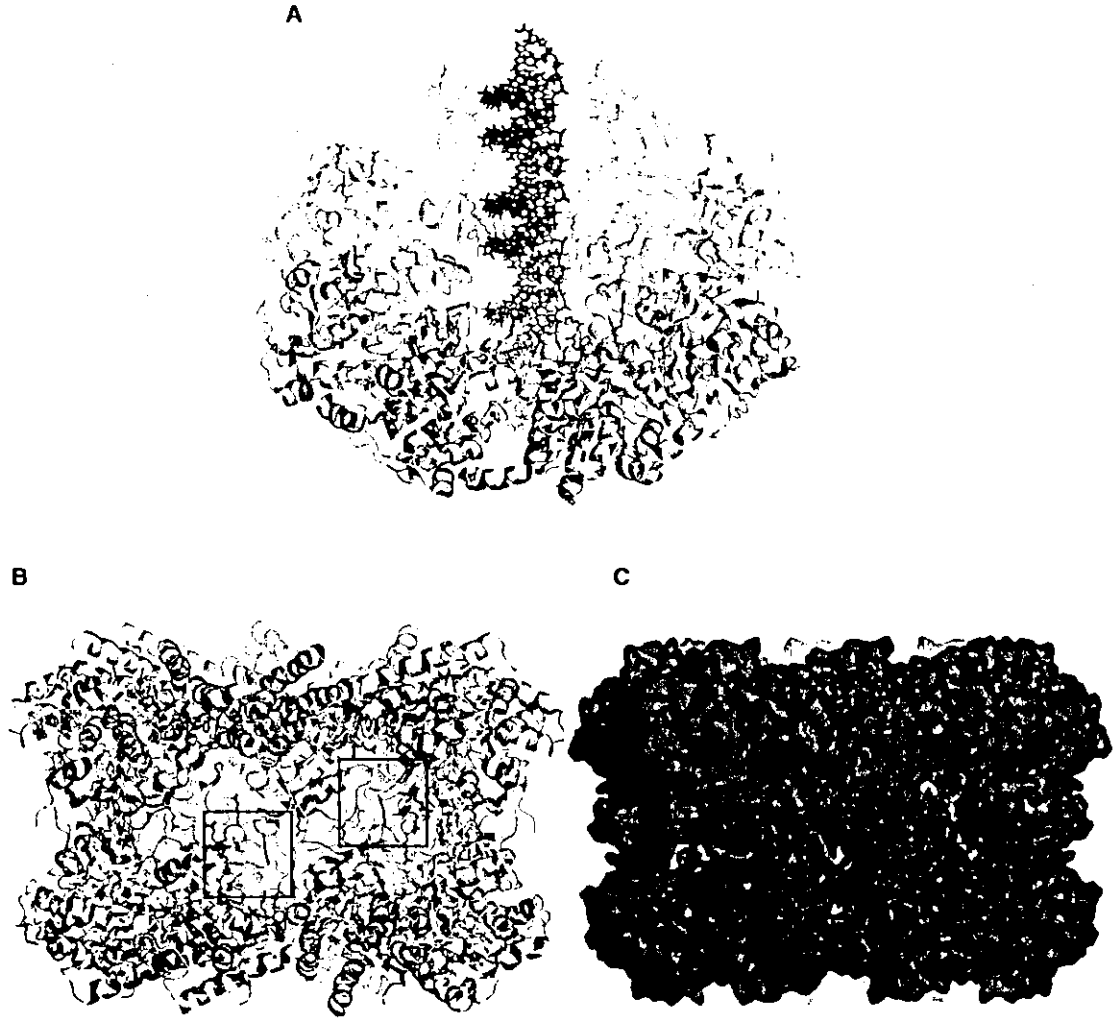

Figure 5. The DNA Binding Sites of Dmc1

(A) The dsDNA passes through the central channel of Dmc1. The same side chains as in Figure 3C are shown. (B) Double ring formation by Dmc1. (C) Electrostatic surface potential of the Dmc1 double ring structure, viewed from the side. Positively charged cavities are boxed in (B) and (C), and contain an amino acid residue (R311) essential for ssDNA binding.

By a combination of surface potential calculations and mutational analyses, we obtained information about how Dmc1 may bind to ssDNA and dsDNA to promote homologous pairing. The dsDNA molecule is likely to pass through the central channel of the ring, which is large enough to accommodate B form duplex DNA (Figure 5A) and displays the inner basic patches that contain residues essential for dsDNA binding (Figures 3B and 3D). The dsDNA binding through the central channel of the stacked Dmc1 rings was previously observed by electron microscopy (Passy et al., 1999).

On the other hand, two specific ssDNA binding residues were found at separate locations on the Dmc1 octamer surface. One is Phe233 at the Loop 1 region (the inner basic patch), which also displays dsDNA binding residues, on the central channel of the ring (Figures 3B and 3D). The other is Arg311, in the outer basic patch at the perimeter of the ring (Figures 3B and 3E). The Arg311 residue is located at the entrance of the cavity formed at the Dmc1 monomer-monomer interface (Figures 5B and 5C). This cavity is large enough to accommodate an ssDNA molecule, but not a dsDNA molecule (Figures 5B and 5C). Dmc1 may therefore spool the ssDNA molecule through the cavity located on the side of the stacked Dmc1 rings. The dsDNA and ssDNA binding modes of Dmc1 starkly contrast with the proposed ternary complex formation modes of the Rad51 protein (Shin et al., 2003) and the human Rad52 protein (Kagawa et al., 2001, 2002; Singleton et al., 2002). This suggests that eukaryotes have evolutionarily acquired several proteins promoting the homologous-pairing reaction through different DNA binding modes.

The Dmc1 ring must be open to allow the intact dsDNA to pass through its central channel. Our biochemical studies showed that Dmc1 did not require ATP for dsDNA binding (data not shown), and the previous electron microscopic studies revealed that the stacked Dmc1 rings are formed around the dsDNA in the absence of ATP (Passy et al., 1999). Hence, it appears that the opening of the Dmc1 ring does not require ATP hydroly-

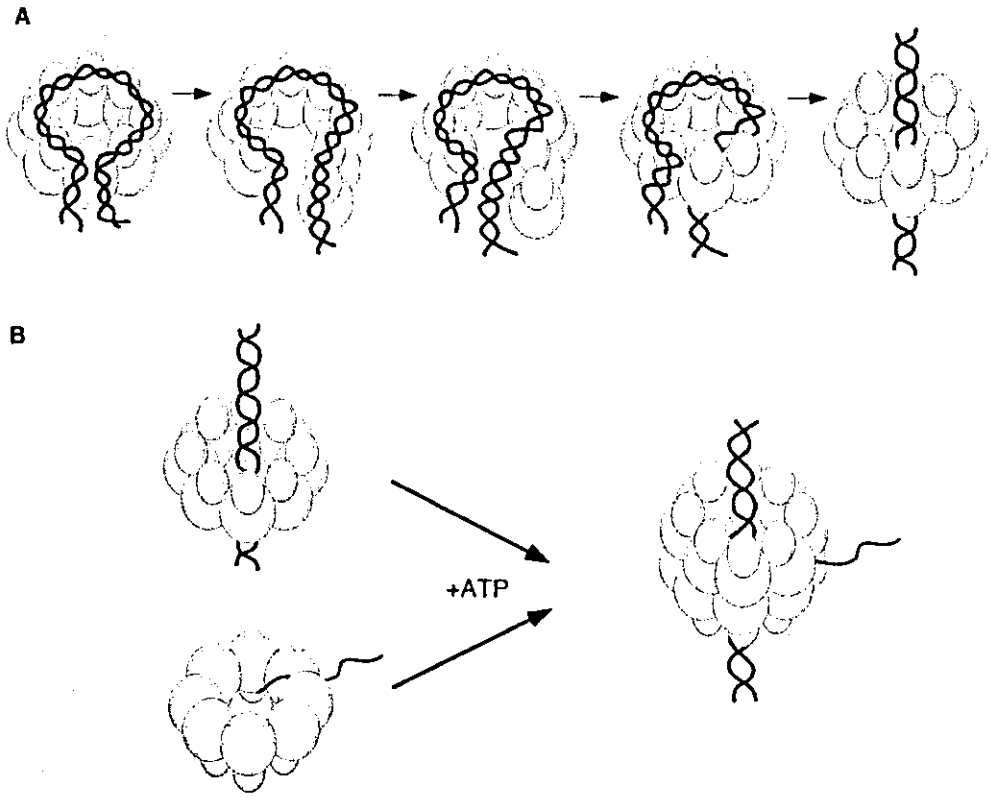

Figure 6. A Model of a Homologous Pairing Intermediate Complex between Dmc1, ssDNA, and dsDNA

(A) Schematic representation of dsDNA passing through the central channel of Dmc1. The N-terminal domain (colored yellow) may initially bind to dsDNA, creating a bending stress that could cause the dissociation of the ATPase domain (colored pink).

(B) Ternary complex formation by the Dmc1 double ring, ssDNA, and dsDNA requires ATP. The search and the pairing of two homologous sequences could take place at the center of the Dmc1 double ring. The dsDNA is shown entering from one end of the stacked ring. The ssDNA is shown passing through the cavity created by the stacking of two Dmc1 rings.

sis. Then, how does dsDNA binding disrupt the ring? For the Dmc1 ring to open up, the interaction between the polymerization motif (β0) and the adjacent monomer needs to be disrupted. Just upstream of the polymerization motif (β0) is the N-terminal domain, and its counterpart in the human Rad51 protein was shown to bind dsDNA (Aihara et al., 1998). In the process of binding to dsDNA, the N-terminal domain of Dmc1 would impose bending stress on the dsDNA (Figure 6A), and this energy may promote the disruption of the interaction between the polymerization motif (β0) and the adjacent monomer, thus allowing the bound dsDNA molecule to enter into the central channel (Figure 6A). Another possibility is that the Dmc1 octamer is temporarily converted to a helical filament by the exchange of monomer-monomer interactions between adjacent rings. Such opening of ring-structured proteins has been demonstrated in studies of the T7 gene 4 helicase (Sawaya et al., 1999; Toth et al., 2004).

On the basis of the ssDNA and dsDNA binding paths on the Dmc1 double ring, we have developed a model for the ternary complex, including the Dmc1 double ring, ssDNA, and dsDNA (Figure 6B). The center of the Dmc1 double ring is probably the catalytic site for the search and exchange of DNA strands (Figure 6B). The Loop 2 region, which was disordered in the crystal structure, is located within this region, and could play an important, yet unknown, role. The bipolar nature of the stacked Dmc1 rings is suited for a bidirectional homology search, which is an important factor for efficient homologous pairing. In contrast to the ssDNA and dsDNA binding by Dmc1, the formation of the ternary complex was absolutely dependent on ATP (Figure 4E). Therefore, ATP is likely to play an essential role in ternary complex formation. The ATP binding site (Walker B motif) of Dmc1 is located near the entrance of the cavity that is proposed to bind the ssDNA molecule. Hence, the binding of ATP may play an essential role in transporting the ssDNA molecule in the ternary complex, perhaps by inducing conformational changes in the monomer structure, as in the T7 gene 4 helicase (Singleton et al., 2000) and the replicative helicase of large T antigen (Li et al., 2003). Further insights into the Dmc1-promoted homologous pairing will await structural studies on the Dmc1 protein bound to ATP and/or DNA.

Experimental Procedures

Protein Purification

The human Dmc1 gene was inserted into the pET-15b plasmid (Novagen), and the protein was overexpressed in the *E. coli* strain BL21(DE3) Codon Plus (Stratagene) as a N-terminal hexahistidine-tagged protein. Dmc1 was purified from a 10 liter LB culture incu-

bated at 30°C. When the OD_{600} of the culture was between 0.4–0.6, the protein expression was induced by adding IPTG to a final concentration of 1 mM. Cells were harvested after an overnight incubation, and were lysed by sonication in buffer A (50 mM Tris-HCl buffer [pH 8.0] containing 0.5 M NaCl, 10 mM 2-mercaptoethanol, 10% glycerol, and protease inhibitors [Complete EDTA-free; Roche Molecular Biochemicals]) on ice. The cell lysate was centrifuged at 27,700 × *g* for 20 min, and the supernatant was gently mixed by the batch method with 4 ml of Ni-NTA agarose beads (Qiagen) for 1 hr. The protein-bound beads were packed into an Econo-column (Bio-Rad) and were washed with 30 column volumes of buffer A containing 5 mM imidazole. The Dmc1 protein was eluted in a 20 column volume linear gradient of 5 mM to 300 mM imidazole in buffer A. The peak fractions, which predominantly contained Dmc1, were collected and thrombin protease (3 units per mg of Dmc1; Amersham Biosciences) was added to cleave off the His-tag. The thrombin-containing fractions were immediately dialyzed overnight at 4°C in buffer B (50 mM Tris-HCl buffer [pH 8.0] containing 0.2 M KCl, 0.5 mM EDTA, 10 mM 2-mercaptoethanol, and 10% glycerol). The protein, which now lacked the His-tag, was subjected to chromatography on a 4 ml Heparin-Sepharose (Amersham Biosciences) column. The column was washed with 20 column volumes of buffer B, and the protein was eluted with a 20 column volume linear gradient of 0.2 M to 1.2 M KCl in buffer B. The Dmc1 protein was eluted in a sharp peak at about 0.7 M KCl. The protein concentration was determined using the Bio-Rad protein assay kit, with bovine serum albumin (Pierce) as the standard. The pET-15b expression vectors for the nine Dmc1 point mutants (R230A, F233A, R236A, R242A, E258A, R304A, K305A, R307A, and R311A) were constructed using the QuikChange mutagenesis kit (Stratagene). All mutants were purified by the aforementioned procedure.

Crystallization

Dmc1 crystals were grown by the hanging drop method at 20°C. The hanging drop was formed by adding 1 μl of Dmc1 (concentrated to 8 mg/ml) to 1 μl of the reservoir solution (0.1 M sodium citrate buffer [pH 5.8] containing 50 mM $MgCl_2$ and 8% PEG 2000 MME). Crystals typically appeared after 1 week, and reached the maximum size (0.5 mm × 0.5 mm × 0.05 mm) after 2 weeks. For data collection, the Dmc1 crystals were harvested in a reservoir solution containing 30% PEG 400, and were flash-frozen in a stream of N_2 gas (100 K). The data set of the crystal was collected at the SPring-8 BL44B2 beamline (Harima, Japan). The data were reduced using the DENZO and SCALEPACK programs (Otwinowski and Minor, 1997). Crystals of Dmc1 belong to the tetragonal space group of I422 with unit cell dimensions $a = b = 124.06$ Å and $c = 216.37$ Å.

Structure Determination and Refinement

The structure of the human Dmc1 protein was solved by molecular replacement, using the coordinates of the ATPase domain of the human Rad51 structure (Protein Data Bank accession number 1N0W) as a search model. Using the MOLREP program (CCP4, 1994), rotational and translational searches were performed with the Dmc1 data between 20-4 Å resolution, with a 35 Å integration radius. The solution, which contained two monomers, had a correlation factor of 0.66. All refinements were done using the CNS program (Brunger et al., 1998). The first round of refinement consisted of rigid-body refinement, followed by energy minimization, B-individual refinement and simulated annealing. A 2-fold NCS restraint (imposed on the two Dmc1 monomers in the asymmetric unit) was included in all refinements after the rigid-body refinement, which gave an *R* factor of 0.45. The $2|F_o|-|F_c|$ map calculated after simulated annealing contained clearly interpretable ATPase domains. Iterative rounds of model building using the O program (Jones et al., 1991) and refinement (energy minimization, B-individual refinement, and simulated annealing) were performed to build on unmodeled portions of the electron density maps. In this process, the $|F_o|-|F_c|$ maps were calculated to help determine the side chain conformations that were not clear in the initial electron density maps. In the final round of refinement, B-group refinement was done instead of B-individual refinement. The Ramachandran plot of the final structure showed 81.2% of the residues in the most favorable regions, and no residues in the disallowed region. All structure figures were created using the PyMOL program (DeLano, 2002).

Analytical Ultracentrifugation

Sedimentation equilibrium experiments were performed in a Beckman Optima XL-I instrument. Dmc1 (0.5 mg/ml) was spun in a Beckman An-60Ti rotor with a 6-sector centerpiece. The protein was extensively dialyzed against 10 mM Tris-HCl buffer (pH 8.0) containing 50 mM KCl, 0.5 mM EDTA, 2 mM 2-mercaptoethanol, and 10% glycerol. Equilibrium distributions were analyzed after 18 hr of centrifugation at 9,000 rpm and 20°C. For the molecular weight analysis, a partial specific volume of 0.675 cm^3/g and a solution density of 1.05 g/cm^3 were used.

CD Measurements

CD spectra of the wild-type Dmc1 and the E258A mutant (both at 4 μM) were recorded on a JASCO J-820 spectropolarimeter (Japan Spectroscopic Co., Ltd.). All CD experiments were performed in a buffer containing 20 mM phosphate (pH 7.0) and 50 mM KCl.

Assay for DNA Binding

All reaction mixtures contained final buffer concentrations of 20 mM Tris-HCl (pH 8.0), 1 mM $MgCl_2$, 0.1 mg/ml BSA, 2 mM creatine phosphate, and 75 μM creatine phosphokinase. The indicated amounts of Dmc1 were incubated with 1 μM of SAT-1 ssDNA (5′ ATT TCATGCTAGACAGAAGAATTCTCAGTAACTTCTTTGTGCTGTGTG TGTA 3′) for 6 min at 37°C. The Dmc1-ssDNA complexes were then fixed with 0.04% glutaraldehyde for 20 min. Complexes were resolved by 1% agarose gel electrophoresis in 0.5 × TBE buffer at 3.3 V/cm for 2.5 hr, and were visualized by autoradiography of the dried gel. Products and reactants were visualized using a Fuji BAS2500 image analyzer. For the dsDNA binding assay, 10 μM of ϕX174 DNA, linearized with PstI, was incubated with the indicated amounts of Dmc1 for 5 min at 37°C. Complexes were resolved by 1% agarose gel electrophoresis in 0.5 × TBE buffer at 3.3 V/cm for 2.5 hr, and were visualized by ethidium bromide staining. All DNA concentrations are expressed in moles of nucleotides.

Assays for Ternary Complex and D Loop Formation

In both assays, the reactions were started by incubating the indicated amounts of Dmc1 with 1 μM of SAT-1 ssDNA for 5 min. Afterwards, the supercoiled pGsat4 (3,218 bp) DNA (final concentration of 30 μM) was added along with $MgCl_2$ (final concentration of 10 mM). The reaction mixtures were further incubated for 10 min. To observe the ternary complexes, glutaraldehyde was added to a final concentration of 0.04%, and the mixtures were incubated for 20 min. To observe the D loops, 1 μl of 5% SDS, followed by 1 μl of 6 mg/ml proteinase K, was added, and the reactions were incubated for 15 min. Both products were resolved by 1% agarose gel electrophoresis in 0.5 × TBE buffer at 3.3 V/cm for 2.5 hr, and were visualized by autoradiography of the dried gel.

Acknowledgments

We thank N. Nakajima, H. Kawano, and N. Kamiya for collecting diffraction data, and R. Ishitani, S.-Y. Park, and H. Yamaguchi for help with structure determination and refinement. This work was supported by the Bioarchitect Research Program (RIKEN), CREST of JST (Japan Science and Technology), the RIKEN Structural Genomics/Proteomics Initiative (RSGI), the National Project on Protein Structural and Functional Analyses, and a Grant-in-Aid from the Ministry of Education, Sports, Culture, Science, and Technology, Japan.

Received: January 26, 2004
Revised: March 30, 2004
Accepted: April 1, 2004
Published: May 6, 2004

References

Aihara, H., Ito, Y., Kurumizaka, H., Yokoyama, S., and Shibata, T. (1998). The N-terminal domain of the human Rad51 protein binds

DNA: structure and a DNA binding surface as revealed by NMR. J. Mol. Biol. *290*, 495–504.

Bashford, D., and Gerwert, K. (1992). Electrostatic calculations of the pKa values of ionizable groups in Bacteriorhodopsin. J. Mol. Biol. *224*, 473–486.

Baumann, P., Benson, F.E., Hajibagheri, N., and West, S.C. (1997). Purification of human Rad51 protein by selective spermidine precipitation. Mutat. Res. *384*, 65–72.

Benson, F.E., Stasiak, A., and West, S.C. (1994). Purification and characterization of the human Rad51 protein, an analogue of *E. coli* RecA. EMBO J. *13*, 5764–5771.

Berendsen, H.J.C., van der Spoel, D., and van Drunen, R. (1995). GROMACS: a message-passing parallel molecular dynamics implementation. Comp. Phys. Comm. *91*, 43–56.

Bishop, D.K., Park, D., Xu, L., and Kleckner, N. (1992). *DMC1*: a meiosis-specific yeast homolog of *E. coli* recA required for recombination, synaptonemal complex formation, and cell cycle progression. Cell *69*, 439–456.

Brunger, A.T., Adams, P.D., Clore, G.M., DeLano, W.L., Gros, P., Grosse-Kunstleve, R.W., Jiang, J.-S., Kuszewski, J., Nilges, M., and Pannu, N.S. (1998). Crystallography and NMR system: a new software suite for macromolecular structure determination. Acta Crystallogr. D *54*, 904–925.

CCP4 (Collaborative Computational Project, Number 4) (1994). The CCP4 suite: programs for protein crystallography. Acta Crystallogr. D *50*, 760–763.

DeLano, W.L. (2002). The PyMOL Molecular Graphics System. DeLano Scientific, San Carlos, California.

Habu, T., Taki, T., West, A., Nishimune, Y., and Morita, T. (1996). The mouse and human homologs of DMC1, the yeast meiosis-specific homologous recombination gene, have a common unique form of exon-skipped transcript in meiosis. Nucleic Acids Res. *24*, 470–477.

Heuser, J., and Griffith, J. (1989). Visualization of RecA protein and its complexes with DNA by quick-freeze/deep-etch electron microscopy. J. Mol. Biol. *210*, 473–484.

Hong, E.L., Shinohara, A., and Bishop, D.K. (2001). *Saccharomyces cerevisiae* Dmc1 protein promotes renaturation of single-strand DNA (ssDNA) and assimilation of ssDNA into homologous supercoiled duplex DNA. J. Biol. Chem. *276*, 41906–41912.

Jones, T.A., Zou, J.-Y., Cowan, S.W., and Kjeldgaard, M. (1991). Improved methods for building protein models in electron density maps and the location of errors in these models. Acta Crystallogr. A *47*, 110–119.

Kagawa, W., Kurumizaka, H., Ikawa, S., Yokoyama, S., and Shibata, T. (2001). Homologous pairing promoted by the human Rad52 protein. J. Biol. Chem. *276*, 35201–35208.

Kagawa, W., Kurmizaka, H., Ishitani, R., Fukai, S., Nureki, O., Shibata, T., and Yokoyama, S. (2002). Crystal structure of the homologous-pairing domain from the human Rad52 recombinase in the undecameric form. Mol. Cell *10*, 359–371.

Kleckner, N. (1996). Meiosis: how could it work? Proc. Natl. Acad. Sci. USA *93*, 8167–8174.

Komori, K., Miyata, T., DiRuggiero, J., Holley-Shanks, R., Hayashi, I., Cann, I.K.O., Mayanagi, K., Shinagawa, H., and Ishino, Y. (2000). Both RadA and RadB are involved in homologous recombination in *Pyrococcus furiosus*. J. Biol. Chem. *275*, 33782–33790.

Li, Z., Golub, E.I., Gupta, R., and Radding, C.M. (1997). Recombination activities of HsDmc1 protein, the meiotic human homolog of RecA protein. Proc. Natl. Acad. Sci. USA *94*, 11221–11226.

Li, D., Zhao, R., Lilyestrom, W., Gai, D., Zhang, R., DeCaprio, J.A., Fanning, E., Jochimiak, J., Szakonyl, G., and Chen, X.S. (2003). Structure of the replicative helicase of the oncoprotein SV40 large tumour antigen. Nature *423*, 512–518.

Lindahl, E., Hess, B., and van der Spoel, D. (2001). GROMACS 3.0: a package for molecular simulation and trajectory analysis. J. Mol. Mod. *7*, 306–317.

Masson, J.Y., and West, S.C. (2001). The Rad51 and Dmc1 recombinases: a non-identical twin relationship. Trends Biochem. Sci. *26*, 131–136.

Masson, J.Y., Davies, A.A., Hajibagheri, N., Van Dyck, E., Benson, F.E., Stasiak, A.Z., Stasiak, A., and West, S.C. (1999). The meiosis-specific recombinase hDmc1 forms ring structures and interacts with hRad51. EMBO J. *18*, 6552–6560.

Miyata, T., Yamada, K., Iwasaki, H., Shinagawa, H., Morikawa, K., and Mayanagi, K. (2000). Two different oligomeric states of the RuvB branch migration motor protein as revealed by electron microscopy. J. Struct. Biol. *131*, 83–89.

Nishinaka, T., Ito, Y., Yokoyama, S., and Shibata, S. (1997). An extended DNA structure through deoxyribose-base stacking induced by RecA protein. Proc. Natl. Acad. Sci. USA *94*, 6623–6628.

Ogawa, T., Yu, X., Shinohara, A., and Egelman, E.H. (1993). Similarity of the yeast RAD51 filament to the bacterial RecA filament. Science *26*, 1896–1899.

Otwinowski, Z., and Minor, W. (1997). Processing of X-ray diffraction data collected in oscillation mode. Methods Enzymol. *276*, 307–326.

Passy, S.I., Yu, X., Li, Z., Radding, C.M., Masson, J.Y., West, S.C., and Egelman, E.H. (1999). Human Dmc1 protein binds DNA as an octameric ring. Proc. Natl. Acad. Sci. USA *96*, 10684–10688.

Pellegrini, L., Yu, D.S., Lo, T., Anand, S., Lee, M., Blundell, T.L., and Venkitaraman, A.R. (2002). Insights into DNA recombination from the structure of a RAD51-BRCA2 complex. Nature *420*, 287–293.

Pittman, D.L., Cobb, J., Schimenti, K.J., Wilson, L.A., Cooper, D.M., Brignull, E., Handel, M.A., and Schimenti, J.C. (1998). Meiotic prophase arrest with failure of chromosome synapsis in mice deficient for Dmc1, a germline-specific RecA homolog. Mol. Cell *1*, 697–705.

Roeder, G.S. (1997). Meiotic chromosomes: it takes two to tango. Genes Dev. *11*, 2600–2621.

Sawaya, M.R., Guo, S., Tabor, S., Richardson, C.C., and Ellenberger, T. (1999). Crystal structure of the helicase domain from the replicative helicase-primase of bacteriophage T7. Cell *99*, 167–177.

Seitz, E.M., Brockman, J.P., Sandler, S.J., Clark, A.J., and Kowalczykowski, S.C. (1998). RadA protein is an archaeal RecA protein homolog that catalyzes DNA strand exchange. Genes Dev. *12*, 1248–1253.

Shin, D.S., Pellegrini, L., Daniels, D.S., Yelent, B., Craig, L., Bates, D., Yu, D.S., Shivji, M.K., Hitomi, C., Arvai, A.S., et al. (2003). Full-length archaeal Rad51 structure and mutants: mechanisms for RAD51 assembly and control by BRCA2. EMBO J. *22*, 4566–4576.

Singleton, M.R., Sawaya, M.R., Ellenberger, T., and Wigley, D.B. (2000). Crystal structure of T7 gene 4 ring helicase indicates a mechanism for sequential hydrolysis of nucleotides. Cell *101*, 589–600.

Singleton, M.R., Wentzell, L.M., Liu, Y., West, S.C., and Wigley, D.B. (2002). Structure of the single-strand annealing domain of human RAD52 protein. Proc. Natl. Acad. Sci. USA *99*, 13492–13497.

Spies, M., Kil, Y., Masui, R., Kato, R., Kujo, C., Ohshima, T., Kuramitsu, S., and Lanzov, V. (2000). The RadA protein from a hyperthermophilic archaeon *Pyrobaculum Islandicum* is a DNA-dependent ATPase that exhibits two disparate catalytic modes, with a transition temperature at 75 degrees C. Eur. J. Biochem. *267*, 1125–1137.

Stasiak, A., DiCapua, E., and Koller, T. (1981). Elongation of duplex DNA by recA protein. J. Mol. Biol. *151*, 557–564.

Stasiak, A., and DiCapua, E. (1982). The helicity of DNA in complexes with recA protein. Nature *299*, 185–186.

Stasiak, A., Stasiak, Z., and Koller, T. (1984). Visualization of RecA-DNA complexes involved in consecutive stages of an in vitro strand exchange reaction. Cold Spring Harb. Symp. Quant. Biol. *49*, 561–570.

Story, R.M., Weber, I.T., and Steitz, T.A. (1992). The structure of the *E. coli* recA protein monomer and polymer. Nature *355*, 318–325.

Symington, L.S. (2003). Role of *RAD52* epistasis group genes in homologous recombination and double-strand break repair. Microbiol. Mol. Biol. Rev. *66*, 630–670.

Toth, E.A., Li, Y., Sawaya, M.R., Cheng, Y., and Ellenberger, T. (2004). The crystal structure of the bifunctional primase-helicase of bacteriophage T7. Mol. Cell *12*, 1113–1123.

Tsang, S.S., Chow, S.A., and Radding, C.M. (1985). Networks of DNA and RecA protein are intermediates in homologous pairing. Biochemistry *24*, 3226–3232.

Yang, S., VanLoock, M.S., Yu, X., and Egelman, E.H. (2001a). Comparison of bacteriophage T4 UvsX and Rad51 filaments suggests that RecA-like polymers may have evolved independently. J. Mol. Biol. *312*, 999–1009.

Yang, S., Yu, X., Seitz, E.M., Kowalczykowski, S.C., and Egelman, E.H. (2001b). Archaeal RadA protein binds DNA as both helical filaments and octameric rings. J. Mol. Biol. *314*, 1077–1085.

Yoshida, K., Kondoh, G., Matsuda, Y., Habu, T., Nishimune, Y., and Morita, T. (1998). The mouse RecA-like gene Dmc1 is required for homologous chromosome synapsis during meiosis. Mol. Cell *1*, 707–718.

Yu, X., and Egelman, E.H. (1997). The RecA hexamer is a structural homologue of ring helicases. Nat. Struct. Biol. *4*, 101–104.

Accession Numbers

The atomic coordinates of the human Dmc1 protein have been deposited in the RCSB Protein Data Bank with the accession code 1V5W.

The EMBO Journal (2004) 23, 670–680 | © 2004 European Molecular Biology Organization | All Rights Reserved 0261-4189/04
www.embojournal.org

THE EMBO JOURNAL

XRCC3 deficiency results in a defect in recombination and increased endoreduplication in human cells

Takashi Yoshihara[1,3], Mari Ishida[1], Aiko Kinomura[1], Mari Katsura[1], Takanori Tsuruga[1], Satoshi Tashiro[2], Toshimasa Asahara[3] and Kiyoshi Miyagawa[1,*]

[1]Department of Human Genetics, Research Institute for Radiation Biology and Medicine, Hiroshima University, Hiroshima, Japan, [2]Department of Biochemistry, Graduate School of Biomedical Sciences, Hiroshima University, Hiroshima, Japan, [3]Department of Surgery, Graduate School of Biomedical Sciences, Hiroshima University, Hiroshima, Japan

XRCC3 was inactivated in human cells by gene targeting. Consistent with its role in homologous recombination, *XRCC3*$^{-/-}$ cells showed a two-fold sensitivity to DNA cross-linking agents, a mild reduction in sister chromatid exchange, impaired Rad51 focus formation and elevated chromosome aberrations. Furthermore, endoreduplication was increased five- seven-fold in the mutants. The T241M variant of XRCC3 has been associated with an increased cancer risk. Expression of the wild-type cDNA restored this phenotype, while expression of the variant restored the defective recombinational repair, but not the increased endoreduplication. RPA, a protein essential for homologous recombination and DNA replication, is associated with XRCC3 and Rad52. Overexpression of RPA promoted endoreduplication, which was partially complemented by overexpression of the wild-type XRCC3 protein, but not by overexpression of the variant protein. Overexpression of Rad52 prevented endoreduplication in RPA-overexpressing cells, in *XRCC3*$^{-/-}$ cells and in the variant-expressing cells, suggesting that deregulated RPA was responsible for the increased endoreduplication. These observations offer the first genetic evidence for the association between homologous recombination and replication initiation having a role in cancer susceptibility.

The EMBO Journal (2004) **23**, 670–680. doi:10.1038/sj.emboj.7600087; Published online 29 January 2004
Subject Categories: genome stability & dynamics
Keywords: DNA damage; endoreduplication; homologous recombination; XRCC3

Introduction

DNA replication frequently stalls when either the template DNA is damaged or the replication machinery malfunctions. The stalled replication forks generate DNA double-strand breaks (DSBs) that are repaired by homologous recombination between sister chromatids (Haber, 1999). Homologous recombination is a high-fidelity repair mechanism that serves to eliminate chromosome aberrations before cell division occurs. Thus, chromosome aberrations are increased in cells lacking homologous recombination proteins, including Rad51, Rad51 paralogs, Rad54, Rad50, Mre11, Nbs1, BRCA1 and BRCA2 (Morrison and Takeda, 2000; Thompson and Schild, 2001). In addition to the general link between replication and recombination, a relationship between recombination and the initiation of replication has been reported in *Schizosaccharomyces pombe* (Segurado *et al*, 2002). The activation of DNA replication origins was associated with the generation of recombination intermediates. The frequency of homologous integration was extremely high at the DNA replication origins. These findings suggest that DNA replication is initiated in the close vicinity of homologous integration hot spots in *S. pombe*.

To ensure that the entire genome of a cell is replicated only once in each cell cycle, replication origins must be strictly regulated. As cells enter G1, replication origins are licensed by proteins such as Cdc6 and the Mcm2–7 complex. These proteins are recruited to the origin recognition complex (ORC) to form a prereplicative complex (Diffley and Labib, 2002). Cdc6 is replaced by Cdc45, which recruits DNA polymerase α-primase and replication protein A (RPA) to the replication origin (Walter and Newport, 2000). Cyclin-dependent kinases (CDKs) have been implicated in preventing the licensing of replicated DNA. In *Saccaromyces cerevisiae*, B-type CDKs prevent endoreduplication through multiple mechanisms, including phosphorylation of the ORC, downregulation of Cdc6 and nuclear exclusion of the Mcm2–7 complex (Nguyen *et al*, 2001). In *S. pombe*, stable association of the mitotic B-type cyclin Cdc13/Cdc2 kinase with the replication origins prevents endoreduplication (Wuarin *et al*, 2002). Despite these advances, there is limited information available regarding a link between DNA repair and endoreduplication.

The *XRCC3* gene, sharing limited sequence homology with *RAD51*, is inactivated in the Chinese hamster ovary (CHO) cell line irs1SF (Tebbs *et al*, 1995; Liu *et al*, 1998). Constitutive expression of the gene confers resistance to DNA-damaging agents in irs1SF. A fluorescence-based assay that efficiently detects chromosomal gene-conversion events in response to DSBs revealed that XRCC3 promotes the repair of DSBs by homologous recombination in irs1SF (Pierce *et al*, 1999). A reduction of sister chromatid exchange (SCE) levels was observed in DT40 cells lacking XRCC3 (Takata *et al*, 2001). Focus formation of Rad51 in the nucleus, induced by treatment with DNA-damaging agents, was impaired in XRCC3-deficient cells (Bishop *et al*, 1998; Takata *et al*, 2001). An increase in chromosome mis-segregation was

*Corresponding author. Department of Human Genetics, Research Institute for Radiation Biology and Medicine, Hiroshima University, 1-2-3 Kasumi, Minami-ku, Hiroshima 734-8553, Japan.
Tel.: +81 82 257 5828; Fax: +81 82 256 7102;
E-mail: miyag@hiroshima-u.ac.jp

Received: 16 July 2003; accepted: 22 December 2003; Published online: 29 January 2004

observed in irs1SF, which was complemented by expression of XRCC3 (Griffin *et al*, 2000). This chromosome instability was associated with increased centrosome numbers and fragmentation of the centrosome. Thus, these findings in irs1SF suggest that XRCC3 plays a role in chromosome stability through its involvement in centrosome integrity (Griffin, 2002).

The Rad51-like proteins form two protein complexes that play roles in homologous recombination (Masson *et al*, 2001, Liu *et al*, 2002). One complex contains Rad51B/Rad51L1, Rad51C/Rad51L2, Rad51D/Rad51L3 and XRCC2 (BCDX2). This complex binds single-stranded DNA and single-stranded gaps in duplex DNA, suggesting that BCDX2 plays a presynaptic role in recombination. The other complex consists of XRCC3 and Rad51C, and may play a role in homologous pairing (Kurumizaka *et al*, 2001). Moreover, XRCC3 may function not only at the initiation of homologous recombination but also at late stages in the resolution of recombination intermediates (Brenneman *et al*, 2002).

A population-based breast cancer case–control study analyzing polymorphisms in several DNA double-strand break repair genes has revealed that the only amino-acid substitution significantly associated with increased risk was XRCC3 T241M (Kuschel *et al*, 2002). This association was also found for melanoma, bladder carcinoma and squamous cell carcinoma of the head and neck (Winsey *et al*, 2000; Matullo *et al*, 2001; Shen *et al*, 2002), while no association was found for lung carcinoma (Butkiewicz *et al*, 2001; David-Beabes *et al*, 2001). This variant protein complements defects in homologous recombination repair in XRCC3-deficient hamster cells, suggesting that the increased cancer risk associated with the variant is not attributable to repair defects (Araujo *et al*, 2002).

The functions of genes involved in homologous recombination are not always conserved throughout evolution (Lim and Hasty, 1996; Tsuzuki *et al*, 1996; Rijkers *et al*, 1998; Yamaguchi-Iwai *et al*, 1998). To determine the role of XRCC3 in human cells, the gene was deleted in the human colon cancer cell line HCT116 because it has normal mitotic and p53-dependent G1 tetraploidy checkpoints (Michel *et al*, 2001). Defects in homologous recombination and increased endoreduplication were observed in *XRCC3*$^{-/-}$ cells. Furthermore, expression of the variant that is associated with increased cancer risk restored only the defective homologous recombinational repair, but not the increased endoreduplication. RPA was physically associated with XRCC3 and Rad52. RPA-overexpressing cells exhibited the same phenotype as the mutant expressing the variant XRCC3 protein, which was complemented by overexpression of the wild-type XRCC3 protein but not by overexpression of the variant protein. Rad52 prevented endoreduplication in cells overexpressing RPA, in *XRCC3*$^{-/-}$ cells, and in the mutant expressing the variant XRCC3 protein. This observation suggests that endoreduplication resulting from altered XRCC3 function is associated with RPA dysfunction.

Results

Generation of human XRCC3$^{-/-}$ *cells*

The human *XRCC3* locus was disrupted by the insertion of promoterless drug-resistance genes (Figure 1A). Five homozygous mutants were obtained from 193 hygromycin-resistant clones (Figure 1B). Western blot analysis showed that no XRCC3 protein was expressed in the homozygous mutant (Figure 1C). In complementation experiments, the human *XRCC3* cDNA was expressed under the control of the MSV enhancer and the MMTV LTR in the homozygous mutant. A high level of XRCC3 expression was achieved in the presence of dexamethasone (Dex) (Figure 1C). However, the cells having high levels of XRCC3 (more than three-fold higher than endogenous levels) did not grow well. Moderate levels of expression comparable to that of endogenous expression were observed even in the absence of Dex. HCT116 cells were heterozygous for the T241M variation (data not shown).

Growth and sensitivity to DNA-damaging agents of XRCC3$^{-/-}$ *cells*

The growth rate of *XRCC3*$^{-/-}$ cells was almost the same as that of wild-type cells (Figure 2A). The doubling time of the cells was 16 h. *XRCC3*$^{-/-}$ cells showed modest sensitivity to mitomycin C (MMC) (two-fold) (Figure 2B), while they showed no significant increase in sensitivity to ionizing radiation (data not shown). They also showed a similar modest sensitivity to cisplatin (two-fold) (data not shown). Expression of the wild-type (Wt) or variant (Var) *XRCC3* cDNA in the mutant restored this phenotype to levels of sensitivity comparable to that in wild-type cells. Thus, XRCC3 was shown to confer resistance to DNA cross-linking agents in human cells.

Homologous recombination in XRCC3$^{-/-}$ *cells*

A reduction of SCE levels is the hallmark of a defect in sister chromatid-based recombination, and has been observed in DT40 cells lacking homologous recombination proteins, including Rad51 paralogs (Sonoda *et al*, 1999; Takata *et al*, 2001). *XRCC3*$^{-/-}$ cells showed a mild reduction of the level of MMC-induced SCE ($P<0.0001$, Mann–Whitney *U*-test), which was restored by the expression of the wild-type or variant cDNA (Table I). The frequency of targeted integration reflects that of homologous recombination without the use of sister chromatids. To examine the effect of XRCC3 on targeted integration, we measured the frequency at two independent loci, *RAD54B* and *RAD51C* (Miyagawa *et al*, 2002). No statistically significant difference in the targeted integration frequency between wild-type cells and *XRCC3*$^{-/-}$ cells was observed (Table I), implying that XRCC3 plays a role in homologous recombination specifically by using sister chromatids.

Rad51 focus formation is impaired in XRCC3$^{-/-}$ *cells*

DNA-damaging agents induce focus formation of the Rad51 protein in the nucleus, which is required for homologous recombination (Tashiro *et al*, 2000). A lack of Rad51 focus formation has been reported in cells with defects in homologous recombination (Bishop *et al*, 1998; Takata *et al*, 2001). Therefore, we examined the focus formation of Rad51 in *XRCC3*$^{-/-}$ cells. Distinct foci were observed after irradiation in wild-type cells (7.03 ± 1.90 foci per cell, mean$\pm$s.e.m.) and in the mutant expressing the wild-type (9.41 ± 1.75) or variant cDNA (9.00 ± 1.48), whereas the number of foci was significantly reduced in *XRCC3*$^{-/-}$ cells (2.02 ± 0.79) (Figure 2C). These findings are consistent with the finding that sister chromatid-based recombination mediated by Rad51 is inhibited by the lack of a functional *XRCC3* gene.